Mechanistic Evaluation of Test Data from LTPP Jointed Concrete Pavement Test Sections

PUBLICATION NO. FHWA-RD-98-094

JUNE 1998

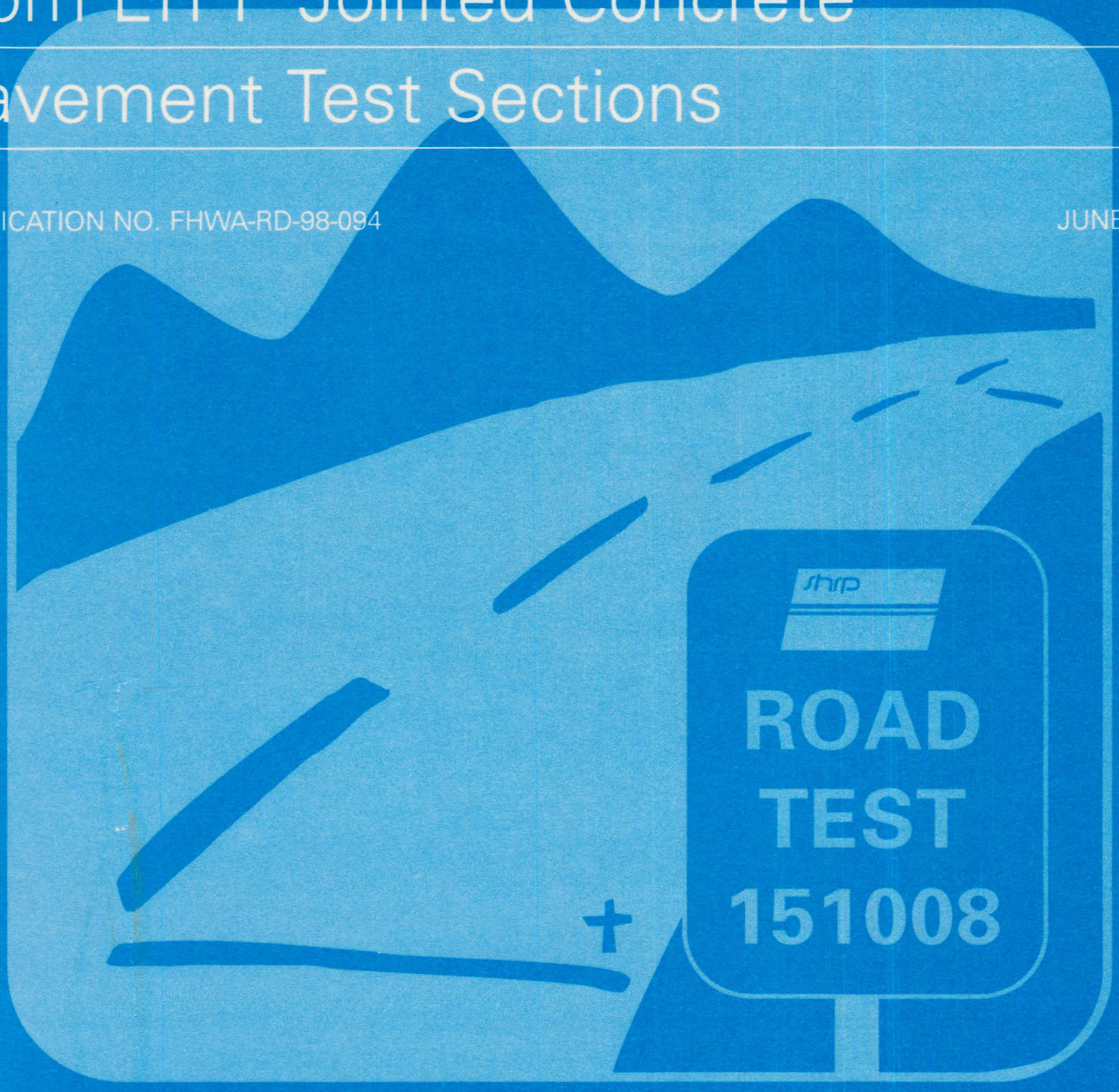

U.S Department of Transportation
Federal Highway Administration

Research and Development
Turner-Fairbank Highway Research Center
6300 Georgetown Pike
McLean, VA 22101-2296

LTPP

FOREWORD

The days in which we can significantly advance the science of pavement engineering through purely empirical approaches are over. Instead, we must turn to mechanistically-based analyses, which seek to explain the mechanisms associated with pavement deterioration. This fact is reflected in the requirement that the 2002 Guide for Design of New and Rehabilitated Pavement Structures (2002 Guide, currently under development through the National Cooperative Highway Research Program) be based on mechanistic concepts.

This report documents the application of Long Term Pavement Performance (LTPP) data to the evaluation of mechanistically-based performance prediction procedures for jointed concrete pavements. It will be of benefit to those interested in the development of mechanistically-based performance prediction and design procedures for jointed concrete pavements. It will be of particular interest to those involved in the development of the 2002 Guide.

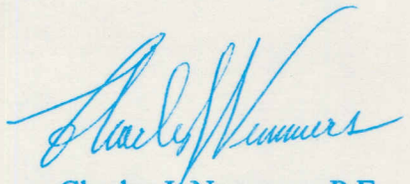

Charles J. Nemmers, P.E.
Director
Office of Engineering
Research and Development

NOTICE

Technical Report Documentation Page

1. Report No.	2. Government Accession No.	3. Recipient's Catalog No.
FHWA-RD-98-094		

4. Title and Subtitle	5. Report Date
MECHANISTIC EVALUATION OF TEST DATA FROM LTPP JOINTED CONCRETE PAVEMENT TEST SECTIONS	June 1998
	6. Performing Organization Code
7. Author(s) Y. Jane Jiang, Shiraz D. Tayabji, and Chung L. Wu	8. Performing Organization Report No.
9. Performing Organization Name and Address ERES Consultants, Inc. 9030 Red Branch Road, Suite 210 Columbia, Maryland 21045	10. Work Unit No. (TRAIS)
	11. Contract or Grant No. DTFH61-95-C-00028
12. Sponsoring Agency Name and Address Office of Research & Development Federal Highway Administration 6300 Georgetown Pike McLean, Virginia 22101-2296	13. Type of Report and Period Covered Final Report Feb 1995 - Dec 1997
	14. Sponsoring Agency Code

15. Supplementary Notes

FHWA Contracting Officer's Technical Representative (COTR): Cheryl Allen Richter, HNR-30
The faulting analysis was performed by Construction Technology Laboratories (CTL), Skokie, Illinois, under a subcontract to ERES. Dr. Chung L. Wu served as the Project Manager and Mr. Paul Okamoto served as the Administrator of the CTL subcontract.

16. Abstract

This study was conducted to assess how well some of the existing concrete pavement mechanistic-empirical based distress prediction procedures performed when used in conjunction with the data being collected as part of the national Long-Term Pavement Performance (LTPP) program. As part of the study, appropriate data were obtained from the National Information Management System (NIMS) for the GPS-3 and GPS-4 experiments. Structural analysis was performed for up to 140 axle load configurations for the selected test sections. Then, ILLICON and the Portland Cement Association (PCA) procedures were used to predict fatigue cracking and joint faulting damage, respectively. The computed results were compared with observed values.

This study has shown that, even given the many current limitations in the LTPP database, the LTPP data can be used successfully to develop better insight into pavement behavior and to improve pavement performance.

17. Key Words	18. Distribution Statement
Concrete pavement, fatigue cracking, joint faulting, LTPP, mechanistic-empirical procedures, NIMS, pavement distress, pavement performance, pavement testing, structural analysis.	No restrictions. This document is available to the public through the National Technical Information Service, Springfield, Virginia 22161.

19. Security Classification (of this report)	20. Security Classification (of this page)	21. No. of Pages	22. Price
Unclassified	Unclassified	77	

Form DOT F 1700.7 (8-72) Reproduction of completed page authorized

SI* (MODERN METRIC) CONVERSION FACTORS

APPROXIMATE CONVERSIONS TO SI UNITS

Symbol	When You Know	Multiply By	To Find	Symbol
	LENGTH			
in	inches	25.4	millimeters	mm
ft	feet	0.305	meters	m
yd	yards	0.914	meters	m
mi	miles	1.61	kilometers	km
	AREA			
in^2	square inches	645.2	square millimeters	mm^2
ft^2	square feet	0.093	square meters	m^2
yd^2	square yards	0.836	square meters	m^2
ac	acres	0.405	hectares	ha
mi^2	square miles	2.59	square kilometers	km^2
	VOLUME			
fl oz	fluid ounces	29.57	milliliters	mL
gal	gallons	3.785	liters	L
ft^3	cubic feet	0.028	cubic meters	m^3
yd^3	cubic yards	0.765	cubic meters	m^3
NOTE: Volumes greater than 1000 l shall be shown in m^3.				
	MASS			
oz	ounces	28.35	grams	g
lb	pounds	0.454	kilograms	kg
T	short tons (2000 lb)	0.907	megagrams (or "metric ton")	Mg (or "t")
	TEMPERATURE (exact)			
°F	Fahrenheit temperature	5(F-32)/9 or (F-32)/1.8	Celcius temperature	°C
	ILLUMINATION			
fc	foot-candles	10.76	lux	lx
fl	foot-Lamberts	3.426	candela/m^2	cd/m^2
	FORCE and PRESSURE or STRESS			
lbf	poundforce	4.45	newtons	N
lbf/in^2	poundforce per square inch	6.89	kilopascals	kPa

APPROXIMATE CONVERSIONS FROM SI UNITS

Symbol	When You Know	Multiply By	To Find	Symbol
	LENGTH			
mm	millimeters	0.039	inches	in
m	meters	3.28	feet	ft
m	meters	1.09	yards	yd
km	kilometers	0.621	miles	mi
	AREA			
mm^2	square millimeters	0.0016	square inches	in^2
m^2	square meters	10.764	square feet	ft^2
m^2	square meters	1.195	square yards	yd^2
ha	hectares	2.47	acres	ac
km^2	square kilometers	0.386	square miles	mi^2
	VOLUME			
mL	milliliters	0.034	fluid ounces	fl oz
L	liters	0.264	gallons	gal
m^3	cubic meters	35.71	cubic feet	ft^3
m^3	cubic meters	1.307	cubic yards	yd^3
	MASS			
g	grams	0.035	ounces	oz
kg	kilograms	2.202	pounds	lb
Mg (or "t")	megagrams (or "metric ton")	1.103	short tons (2000 lb)	T
	TEMPERATURE (exact)			
°C	Celcius temperature	1.8C + 32	Fahrenheit temperature	°F
	ILLUMINATION			
lx	lux	0.0929	foot-candles	fc
cd/m^2	candela/m^2	0.2919	foot-Lamberts	fl
	FORCE and PRESSURE or STRESS			
N	newtons	0.225	poundforce	lbf
kPa	kilopascals	0.145	poundforce per square inch	lbf/in^2

* SI is the symbol for the International System of Units. Appropriate rounding should be made to comply with Section 4 of ASTM E380.

(Revised September 1993)

TABLE OF CONTENTS

TABLE OF CONTENTS
(continued)

Section **Page**

LIST OF FIGURES

LIST OF TABLES

CHAPTER 1 - INTRODUCTION

Over the years, pavement engineers have been attempting to develop "rational" design procedures for both flexible and rigid pavements. These rational procedures have focused on using mechanistic considerations to explain the behavior of pavements under traffic and environmental loadings. The basic assumption of these rational procedures is that the primary pavement distresses are a result of damage induced by the state of stress, strain, or deformation that result from traffic and environmental loadings. Under normal operating conditions, damage to the pavement occurs from a large number of repetitive traffic and environmental loadings over a period of time. Thus, each incremental loading results in some damage to the pavement, and the cumulative effect of the damage over a period of time results in the manifestation of specific distress, for example, fatigue cracking in asphalt concrete (AC) and portland cement concrete (PCC) pavements, rutting in AC pavements, and faulting in PCC pavements. A pavement is considered to have failed when the distress level (severity and extent or magnitude) reaches or exceeds a predefined acceptable level for that distress for a given category of the highway.

Since the 1950's, as techniques for analysis of pavement response to loading began to be available, many attempts have been made to develop these rational design procedures, now commonly referred to as mechanistic-empirical (M-E) procedures, to define/describe the development of specific distresses in pavements. During the late 1980's, extensive evaluation was performed of M-E procedures as part of the National Cooperative Highway Research Program (NCHRP) 1-26 study. In addition, the proposed revision of the *AASHTO Guide for Design of Pavements* to be completed by 2002 will be based on M-E procedures. The M-E procedures typically involve the following steps:

1. Establishing a hypothesis for the mechanism for the development of the specific distress. For example, the development of fatigue cracking in PCC pavements is considered by many to be due to repeated application of bottom tensile strain in the PCC layer. This first step is the most critical because all the subsequent steps depend on the correctness of the hypothesis. The hypothesis determines the type of analysis that needs to be conducted to compute the critical response(s) and the material characterization and traffic characterization needed as input for the analysis.

2. Comprehensively characterizing materials by incorporating changes in material properties as a function of the state of stress (stress dependency), environmental conditions (temperature and moisture), aging, and continual deterioration under traffic loading.

3. Determining critical responses (stresses, strains, deformations) within the pavement layers when subjected to traffic and environmental loadings.

4. Estimating damage from each "set/condition" of traffic and environmental loading. This is typically done using distress prediction models or transfer functions that relate a critical structural response to distress-specific damage. A different model is used for each different distress and for each pavement type.

5. Accumulating the damage over a period of time. Miner's hypothesis is generally used to account for cumulative damage. Based on predefined relationships between the accumulated damage and amount of distress development, the amount of distress that may develop at the end of the selected service life is estimated. At this time, the selected pavement may be redesigned if the estimated amount of distress exceeds the acceptable level or is significantly less than the acceptable level.

6. Selecting as a candidate design a pavement section that results in acceptable levels of distresses at the end of the target service/design life. More than one section may be identified as candidate designs.

Although the above steps seem simple enough, the actual process is very complex because of many still-undefined factors associated with pavement design and construction, traffic loading, and environmental conditions.

As part of a Federal Highway Administration (FHWA) sponsored project, work was undertaken to use test data from the on-going Long-Term Pavement Performance (LTPP) program in conjunction with currently available M-E design procedures to assess how well these M-E procedures perform. In essence, the LTPP test data were used to perform a reality check on the validity of several M-E based distress prediction procedures. Under this study, existing M-E design procedures were used to determine cumulative damage in relation to a specific distress in each applicable LTPP test section. The estimated distress was compared with predicted distress. In addition, an attempt was made to develop calibrated distress models that relate the accumulated damage to the observed level of distress.

This report presents the results of the study applicable to jointed PCC test sections from the LTPP program. In the subsequent sections, details are presented on the LTPP program, the LTPP data used in the study, and the procedures undertaken to compute the cumulative damage.

The LTPP Program

The LTPP program is a 20-year program established under the now-completed Strategic Highway Research Program (SHRP). The first 5 years of the LTPP program (mid-1987 to mid-1992) were funded under the SHRP funding; since mid-1992, FHWA has assumed the management and funding of the LTPP program. Although the LTPP program was conceived to meet many needs of the pavement engineering community, one major objective was to develop a national pavement performance data base that could be used to develop and/or validate pavement design procedures. The study reported here was aimed at fulfilling that objective.

The LTPP program is collecting information on the long-term performance of various pavement structures under a range of traffic loadings, climatic factors, and subgrade soils. The LTPP program includes two fundamental classes of studies: the General Pavement Studies (GPS) and the Specific Pavement Studies (SPS). The GPS experiments are a series of selected in-service pavement studies structured to develop a comprehensive national pavement performance data base. These studies are restricted to pavements that incorporate materials and

designs representing good engineering practice and that are in common use across the United States and Canada. Studies included in GPS are:[1]

First Performance Period

GPS-1 - Asphalt Concrete (AC) on Granular Base
GPS-2 - AC on Bound Base
GPS-3 - Jointed Plain Concrete
GPS-4 - Jointed Reinforced Concrete
GPS-5 - Continuously Reinforced Concrete

Overlays

GPS-6 - AC Overlays on AC
GPS-7 - AC Overlays on Portland Cement Concrete Pavements
GPS-9 - Unbonded PCC Overlays on PCC Pavements

Specific details on the GPS-3 and GPS-4 experiments as pertaining to the study reported here are provided in later sections of the report. The SPS program involves the study of specially constructed, maintained, or rehabilitated pavement sections incorporating a controlled set of experimental design and construction features. Test data from the SPS experiments were not included in this study. As such, no additional discussion on the SPS experiments is provided here.

As part of the LTPP program, an extensive data collection effort has been under way since about 1989. These data types are classified within the LTPP program as follows:

1. Inventory
2. Materials Testing
3. Climatic
4. Monitoring
5. Traffic
6. Seasonal

In addition, as appropriate, maintenance, rehabilitation, and construction data are also collected.

Fundamentals of M-E Distress Modeling

The M-E distress modeling approach for PCC pavements involves the following elements:

1. A structural analysis model that can consider the geometry of the pavement, the loading condition (multiple wheel loads), and load transfer effectiveness at joints and that is capable of reliably determining the critical responses appropriate to the distress being considered. For PCC pavements, most of the M-E distress model work has been done using plate on elastic (liquid or Winkler) foundation approach.

2. A fairly reliable estimate of traffic loading. Advanced M-E procedures consider the axle loading spectra while other models are based on use of equivalent loading (e.g., ESAL) in which case all loadings are transformed into a single load type using load equivalency concepts. The use of equivalent traffic loading limits the usefulness of many of these models in developing rational design procedures.

   The traffic loading data may need to be available on a seasonal basis and, in the case of concrete pavements, on a diurnal basis as well as by lateral placement along the width of the traffic lane.

3. A fairly reliable estimate of seasonal climatic conditions to account for changes in material properties and, in the case of concrete pavements, to also account for the effect of temperature differentials within the concrete slab on curling stresses.

4. Comprehensive material characterization. The PCC material properties need to be characterized in terms of aging. For PCC materials, seasonal effects are not considered. The granular material properties need to be characterized in terms of stress dependency and in terms of seasonal variation as a result of seasonal moisture and temperature variations within these materials. For example, the spring-thaw characterization for fine-grained materials is very important.

5. Availability of "calibrated" mechanistic distress models or transfer functions that incorporate mechanistic responses. The general approach has been to develop "absolute" models based on laboratory testing and laboratory failure criteria and to extrapolate these laboratory models to field conditions using a shift factor to account for different levels of distress development and other unaccountable factors. For example, for PCC fatigue cracking, early models were developed on the basis of laboratory testing and the first crack initiation as the failure criterion. These models were then expanded to account for field observations and to incorporate different levels of fatigue cracking (e.g., in terms of number of slab panels exhibiting cracking).

6. Acceptance of Miner's fatigue damage hypothesis. Miner's hypothesis allows a method for combining various levels of damage from the combination of traffic and environmental loadings. Miner's hypothesis states that the structural fatigue damage is cumulative and that a structure's fatigue life is finite, defined by the allowable number of load applications prior to failure. Each load application consumes a small amount of fatigue life. When the actual load applications equal the number of allowable load applications, the fatigue damage is 1.0 or 100 percent and failure occurs. Miner's hypothesis is typically stated as follows:

$$Fatigue\ Damage,\ D_f = \sum \frac{n_i}{N_i} \qquad (1)$$

where: D_f = Cumulative fatigue damage.
n_i = Actual number of load applications of load group i.
N_i = Allowable number of load applications to failure of load group i.

In an ideal M-E procedure, damage (in relation to a specific distress) should be determined as follows:

$$Damage_{ijk\ell} = f\left(e_{ijk\ell}\right) \quad \text{and} \quad e_{ijk\ell} = f\left(E_{jk\ell}\right) \tag{2}$$

where: $e_{ijk\ell}$ = Critical structural response in the pavement that is considered to be a predictor of the distress under consideration for the ith axle group at the jth time period of the kth month of the ℓth year.
$E_{jk\ell}$ = Modulus of elasticity of each layer of the pavement system at the jth time period of the kth month of the ℓth year.

Thus, a major consideration in developing and using M-E procedures is the appropriate characterization of $E_{jk\ell}$ for each of the pavement layer. Our capability for realistically modeling pavement behavior has seen much progress in the last few decades. However, the capability to realistically consider material characterization (e.g., $E_{jk\ell}$) for the pavement layers remains less than desired because of the lack of knowledge on how to realistically account for seasonal effects, spatial variability, and effects of deterioration due to traffic loading and environment.

It should be noted that the above steps are applicable for use of the M-E distress models for design of new/rehabilitated pavements or for checking such designs. The application of the M-E distress models to existing pavements to further validate/calibrate the models creates an entirely different set of problems. Such an effort requires very reliable data on material properties, pavement section layering, past traffic loading history, past environmental conditions, and distress manifestation.

The validation/calibration process involves predicting cumulative damage or distress and comparing the predicted distress to observed distress. The study reported here was aimed at validating or calibrating the distress prediction models for transverse fatigue cracking in jointed plain PCC pavements and for faulting in jointed PCC pavements.

Scope of Work

The overall objective of the study was to assess how well some of the existing M-E based distress prediction procedures performed when used in conjunction with the LTPP data. Specifically, it was decided to assess the transverse cracking prediction procedure developed at the University of Illinois as part of the NCHRP 1-26 study and the joint faulting prediction procedure developed by the Portland Cement Association.

The scope of work included the following for GPS-3 and GPS-4 experiments

- Use of deflection data to backcalculate the pavement layer moduli — an important input to structural evaluation. The base/subbase/subgrade was modeled as a liquid foundation and was therefore characterized in terms of the modulus of subgrade reaction, *k*.

- Use of an algorithm based on finite-element analysis of jointed slabs on elastic foundation to calculate the critical responses. The horizontal tensile strain at the bottom of the PCC layer at mid-slab edge was used as a predictor of fatigue cracking and the deflections at joints were used as a predictor of rutting. Pavement response was calculated for each load level and axle category.

- Existing transfer functions (those developed by the University of Illinois and the Portland Cement Association) were then used to predict the damage associated with each load level. The damage was summed over all load groups and over the entire service life of the pavement. The resulting total damage was then compared with the observed pavement distresses to ascertain if there was a reasonable agreement between the observed and predicted distress levels.

Report Organization

As discussed, this study was aimed at using LTPP data to assess the applicability of several existing M-E analysis procedures. Specifically, the University of Illinois procedure for predicting the development of fatigue cracking and the Portland Cement Association procedure for predicting the development of faulting in jointed PCC pavements were considered. Chapter 2 details the process used to develop the necessary data needed for the study using the LTPP data base. In chapter 3, analysis results are presented for assessment of the University of Illinois (NCHRP 1-26) fatigue cracking prediction procedure. In chapter 4, analysis results are presented for assessment of the Portland Cement Association's joint faulting prediction procedure. Chapter 5 presents a summary of findings and provides a discussion on improvements that need to be made to further advance the reliability of M-E procedures using LTPP data.

CHAPTER 2 - DATA BASE ACQUISITION

The LTPP data used in the analysis reported here were obtained from the National Information Management System (NIMS) during February 1996 (Release 6.0 data). The data were the most recent version of the data release as of the date of this study. The NIMS data are categorized into seven modules: inventory, environment, material testing, monitoring, maintenance, rehabilitation, and traffic. In each module, the data are stored in tables that contain a related set of data elements. This section briefly discusses the data elements used in the analysis, the specific tables from which the data were obtained, the manipulations performed on the data, and the test sections that were excluded from the analysis because of the lack of data.

Inventory/Section Data

Inventory data include general information about each LTPP section, such as section identification, pavement construction date, original design, etc. The key inventory data elements with the corresponding LTPP table names and file extensions used in NIMS are shown in table 1.

Most inventory data variable values were retrieved directly from the NIMS data base except for the slab thickness. If slab thickness data were available from the concrete cores taken from the field, the average core thickness was used. Otherwise, the thickness value from the inventory table was used.

Material Characteristics

The material properties that are typically used in the mechanistic evaluation of transverse fatigue cracking are listed below:

- PCC modulus of elasticity.
- PCC 28-day flexural strength.
- PCC Poisson's ratio.
- PCC coefficient of thermal expansion.
- Stabilized base modulus of elasticity.
- Modulus of subgrade reaction, *k*.

Each data element is described below.

PCC Modulus of Elasticity, E

Backcalculated slab elastic moduli for the LTPP sections were available from a previous study conducted by ERES Consultants, Inc., under FHWA Contract No. DTFH61-94-C-00218. However, because of too many unreasonably high values (greater than 55,000 MPa) from the backcalculation results, these were not used in this study. The following procedure therefore was adopted to estimate the concrete elastic modulus for each section:

1. Obtain the elastic modulus from LTPP data table TST_PC04 (file extension *.T12). The test results were obtained in the laboratory using field cores. This

Table 1. Inventory data elements and the corresponding LTPP tables.

Data Element	LTPP Table Name	File Extension
Section identification information	INV_ID	*.I00
Traffic open date	INV_AGE	*.I04
Slab thickness	TST_PC06 INV_LAYER	*.T2 *.I03
Slab length	INV_PCC_JOINT	*.I06
Slab width	INV_GENERAL	*.I01
28-day flexural strength	TST_PC02 INV_PCC_STRENTH	*.T11 *.I09
PCC slab elastic modulus	TST_PC04 INV_PCC_STRENTH	*.T12 *.I09
Slab Poisson's ratio	TST_PC04	*.T12
Shoulder type	INV_SHOULDER	*.I02
Base type	INV_LAYER	*.I03
Base thickness	INV_LAYER	*.I03

applies to 129 GPS-3 and GPS-4 sections out of the total of 192 GPS-3 and GPS-4 sections.

2. If laboratory test results were not available, then the elastic modulus was extrapolated using the 28-day flexural strength values obtained from the table INV_PCC_STRENGTH (file extension *.I09). Fifteen sections fall into this category.

3. If neither of the above two options were available, a value of 27,580 MPa was assigned to the section. This value has typically been used to represent the elastic modulus for pavement concrete. The default value of 27,580 MPa was used for 48 sections.

PCC 28-day Flexural Strength, M_r

The PCC 28-day flexural strength is a very critical variable in mechanistic evaluation of concrete pavements. The following steps, as prioritized, were taken to determine the 28-day concrete flexural strength for each LTPP section:

1. Calculate the M_r from the splitting tensile strength (σ_T) test data in table TST_PC02 (file extension *.T11). M_r is calculated using the following equation:[2]

$$M_{r(test)} = 210 + 1.02(\sigma_T) \quad (3)$$

where: $M_{r(test)}$ = Flexural strength, psi.
σ_T = Splitting tensile strength, psi.

(Note: 1 psi = 6.895 kPa)

and adjusted using the following equation:[3]

$$M_{r(28-days)} = \frac{M_{r(test)}}{1.22 + 0.17 * Log_{10}(T) - 0.05 * [Log_{10}(T)]^2} \quad (4)$$

where: $M_{r(28-days)}$ = Flexural strength at 28 days, psi.
T = Age of the pavement at test, yr.

(Note: 1 psi = 6.895 kPa)

The 28-day flexural strength was calculated for 128 GPS-3 and GPS-4 sections using this approach.

2. Estimate the 28-day flexural strength from the inventory flexural strength data of different ages in table INV_PCC_STRENGTH (file extension *.I09). Typically, the data were for 7 or 14 days. Therefore, 7-day strengths were multiplied by a coefficient of 1.3 in order to estimate the 28-day strength; 14-day strengths were multiplied by 1.1 to estimate the 28-day strength; i.e.[4]

$$M_{r(28\ days)} = M_{r(test,\ 7\ days)} * 1.3 \quad \textbf{(5)}$$

or

$$M_{r(28\ days)} = M_{r(test,\ 14\ days)} * 1.1 \quad \textbf{(6)}$$

where: $M_{r(test,\ 7\ days)}$ = 7-day flexural strength.
$M_{r(test,\ 14\ days)}$ = 14-day flexural strength.

The 28-day flexural strength values were obtained using this method for 28 sections.

3. Estimate the 28-day flexural strength from the inventory compressive strength data at different ages from table INV_PCC_STRENGTH (file extension *.I09). Again, the compressive strength data were normally measured at 7 or 14 days, so 7-day strengths were multiplied by a coefficient of 1.3 to estimate the 28-day compressive strengths and 14-day strengths were multiplied by 1.1 to estimate the 28-day compressive strengths. The 28-day flexural strengths were estimated from the 28-day compressive strengths ($f'c$) by using the following equation:

$$M_{r(28\ days)} = 10 * [f'c]^{0.5} \quad \textbf{(7)}$$

The 28-day flexural strength value was determined for 13 sections using this method.

4. If no data were available, a value of 4.48 MPa was chosen as a default value for the 28-day flexural strength. This applied to 32 GPS-3 and GPS-4 sections. Furthermore, all the data were reviewed for either very high or very low values. Values in the range of 3.45 MPa to 5.52 MPa were considered acceptable for the analysis. Any values outside these limits were not used, and the default value of 4.48 MPa was used for these sections.

Poisson's Ratio of PCC, ν

The following two steps, as prioritized, were taken to estimate the Poisson's ratio of the concrete:

1. Estimate Poisson's ratio of the section from the data in the LTPP test table TST_PC04 (file extension *.T12). If the tested value was greater than 0.20, then 0.20 was used. The minimum Poisson's ratio obtained from the test table was 0.11, which was considered acceptable. The test values were available for 128 GPS-3 and GPS-4 sections.

2 A value of 0.20 was chosen if test data were not available. Sixty four sections fell into this category.

Coefficient of Thermal Expansion (°C), α

The coefficient of thermal expansion is a variable depending on the concrete mix design and the type of aggregate used. As shown in table 2, the coefficient of thermal expansion of the aggregates varies and affects the overall coefficient of thermal expansion of concrete.[4] Generally, the thermal expansion coefficient of the concrete is between $6.3*10^{-6}/°C$ and $13.5*10^{-6}/°C$. Laboratory tested coefficient of thermal expansion values were not available. Also, the aggregate type and cement content values were not available for many sections in the NIMS data base. Therefore, a value of $9.9*10^{-6}/°C$ was assigned to each section.

Table 2. Thermal properties of aggregate.[4]

	Coefficient of Thermal Expansion, $10^{-6}/°C$
Aggregate	
Granite	7-9
Basalt	6-8
Limestone	6
Dolomite	7-10
Sandstone	11-12
Quartzite	11-13
Marble	4-7

Base Elastic Modulus

When the base layer is a stabilized material with an elastic modulus comparable to the elastic modulus of concrete slab (E_{Base}/E_{Slab} >0.1), then the base layer can have an effect on the slab response to load. However, this is not a very critical variable in the transverse cracking evaluation. For this study, base elastic moduli for stiff stabilized base were estimated using the material code and description of the base course from table INV_LAYERS (file extension *.I03), as shown in table 3.

Table 3. Selected elastic moduli for the base layer of GPS-3 sections.

Description	LTPP Code	Elastic Modulus, MPa
Soil Cement	27	1,379
AC Bound Base (dense graded, hot laid, central plant mix)	28	3,103
AC Bound Base (dense graded, cold laid, central plant mix)	29	1,379
AC Bound Base (open graded, hot laid, central plant mix)	31	1,379
Cement-Aggregate Mixture	37	6,895
Lean Concrete (< 3 sacks cement/cy)	38	13,790
Limerock, Caliche (soft carbonate rock)	41	1,379
Pozzolanic-Aggregate Mixture	44	3,448

Modulus of Subgrade Reaction, k

Deflection data were used to backcalculate the dynamic k values in a recently finished LTPP data analysis project.[5] Two methods were used in the project to determine the subgrade k value. One method was the AREA method currently used in the AASHTO *Guide for the Design of Pavement Structures*, by which the slab radius of relative stiffness, ℓ, is estimated as a function of the AREA of the deflection basin. The second method was a best-fit method, which solves for the combination of ℓ and k and produces the best possible agreement between the predicted and measured deflections at each sensor. Several sensor configurations also were considered to investigate the significance of sensor configuration to backcalculation results. The effect of the finite slab size also was corrected for in the backcalculation results.

On the basis of the results of the comparison of the plate load data and other soils data available in the LTPP data base, the AREA method with seven sensor configurations and slab size corrections was selected for estimation of the dynamic k values. The static k values were then estimated by dividing the mean calculated dynamic k values after data screening by 1.97.[5]

LTPP Traffic Data

Traffic data are one of the most important data elements for the mechanistic evaluation of the distress data. To determine the amount of fatigue and faulting damage accumulated at the critical location, the following data items are needed to represent traffic conditions: axle type, axle weight, number of the axle passes, and lateral traffic distribution.

Intensive efforts are being made to obtain quality traffic data for the LTPP studies. Site monitored traffic data for some sections have recently become available, including Automatic Vehicle Classification (AVC) and Weight-In-Motion (WIM) data. Only the WIM data were used in this study. The data relevant to this study are included in the following two tables:

TRF_MONITOR_AXLE_DISTRIB (file extension *.F04)
TRF_MONITOR_BASIC_INFO (file extension *.F01)

The first table provides information on the axle type, axle weight, and the total number of axles passes for the monitoring year; the second table includes the information on the number of days with WIM monitoring in a given year. The total count is extrapolated based on the number of passes on the WIM monitoring days. Some sections had only 1 year of traffic monitoring data, while others had 2 or 3 years of traffic monitoring data. The monitoring year with the highest number of days with WIM data was selected to represent the traffic condition of the section in one specific year. This was generally the last year of the traffic monitoring data available. There are 140 axle load/type categories for each section. The axle categories include single, tandem, tridem, and four-axle assemblies.

For the fatigue cracking evaluation study, a total of 52 jointed plain concrete pavement (JPCP) sections from a total of 129 sections in the GPS-3 experiment had at least 1 day of traffic monitoring data in 1 year. Table 4 provides a list of sections with traffic monitoring data for the year with the highest number of days of WIM data.

Since the traffic data obtained from the LTPP NIMS data base were available only for a few years, the traffic data for the remaining years had to be backcasted to the year when the pavement was opened to traffic in order to estimate the cumulative traffic.

Backcasting Traffic

To calculate the cumulative fatigue damage, the cumulative traffic passes for each axle weight in each axle group were needed. As discussed previously, for the sections with traffic data, only 1 year of monitored data was selected. Therefore, it was necessary to backcast traffic data to the year the section was opened to traffic. In this study, a constant growth factor of 2 percent was assumed for all the sections. The use of the 2 percent growth factor was considered conservative as it results in a higher level of cumulative traffic loading. The following equation incorporating the 2 percent growth factor was used to calculate the estimated traffic at the beginning year for the test section:

$$T_0 = \frac{T_c}{(1 + 0.02)^{n-1}} \quad \textbf{(8)}$$

where: T_0 = Estimated traffic at the time of opening to traffic.
T_c = Traffic for the monitored year.
n = Age at the time of the traffic monitoring year.

Table 4. Summary of the GPS-3 sections with traffic monitoring data.

State	SHRP ID	Traffic Monitoring Year	Number of Days with WIM Data
5	3011	1993	42
6	3030	1992	29
6	3042	1992	66
8	3032	1993	161
12	3804	1993	14
12	3811	1993	14
12	4000	1993	343
12	4057	1993	333
12	4059	1993	315
12	4109	1993	317
12	4138	1993	343
13	3015	1993	6
13	3018	1993	3
18	3002	1993	168
18	3003	1993	227
18	3030	1993	304
18	3031	1993	135
19	3006	1993	59
19	3009	1993	6
19	3028	1993	5
20	3013	1992	5
20	3015	1993	201
21	3016	1993	146
26	3068	1993	318
26	3069	1993	317
27	3003	1993	219
27	3013	1992	362
29	5393	1993	7
31	3018	1993	9
31	3023	1993	9
31	3028	1993	7
31	3033	1993	6
32	3010	1990	20
32	3013	1992	6
32	7084	1992	14
38	3005	1993	168
38	3006	1993	79
40	4160	1993	31
40	4162	1993	29
42	1623	1991	5
42	3044	1993	3
46	3012	1993	130
53	3011	1993	351
53	3013	1993	343
53	3014	1992	314
53	3019	1992	324
53	3812	1993	362
53	3813	1993	365
53	7409	1993	330
83	3802	1993	205
89	3015	1993	125
89	3016	1992	172

Cumulative Traffic Determination

To be consistent with the backcasting approach, a constant growth rate of 2 percent was again assumed to calculate the cumulative traffic at the time of the distress survey. The following equation was used to compute the cumulative traffic:

$$Cumulative\ Traffic\ Passes = T_0 * \frac{[(1 + 0.02)^{n-1} - 1]}{0.02} \quad (9)$$

Example of Traffic Computation

A GPS section was opened to traffic in January 1970 and the last distress survey was conducted in May 1994. In 1990, the LTPP traffic data indicate that a 111.2 kN single axle was counted 1000 times during that year. Assuming that the traffic growth rate is 2 percent, the cumulative numbers of axle applications are computed as follows:

$$1970\ 111.2\ kN\ Single\ Axle\ Loadings,\ T_0 = 1000/(1.02)^{(20-1)}$$
$$= 686\ applications$$

$$Cumulative\ Axle\ Loadings\ to\ 1994 = 686\ [(1.02)^{24.5} - 1]/0.02$$
$$= 21{,}418\ applications$$

Lateral Distribution of Traffic

The knowledge of lateral distribution of trucks in the traffic lane is critical for computing fatigue cracking damage because of the high longitudinal edge stresses that develop when the truck loading is applied at or near the edge. The truck lateral distribution is a function of width of the traffic lane, location of edge stripe, paved or unpaved shoulders, edge restraints such as retaining walls, and the existence of curbs and gutters. Ideally, the lateral distribution should be measured for local conditions. However, this information is not available in the LTPP data base, and the following general approach was taken to consider the lateral distribution of truck traffic.

It was assumed that the lateral wander of truck traffic is normally distributed about the mean wheelpath. Then, the lateral distribution of the trucks was determined by the mean wheel location and the standard deviation of the traffic wander. Studies by Emery in 1975 showed a mean wheel location of 406 to 457 mm from the edge with a standard deviation of 254 mm on rural lane interstate highways.[6] The lateral distribution was shown to be approximately normal.[3] This results in about 10 percent of loads that were within 152 mm of the slab edge. Another study conducted by Benekohal et al. in 1990 showed an average wheel location of 559 mm from the pavement edge with a standard deviation of 213 mm.[7] These results were based on 1,300 observations. This results in about 3 percent of loads that were within 152 mm of the slab edge. For this study, a conservative value of 8 percent of the loads within 152 mm of the slab edge was selected to account for the truck lateral distribution effect. Thus, for fatigue cracking analysis, only 8 percent of the axle loads were considered with the load located right along the slab edge.

Climatic Data

Climate is another important factor that affects pavement performance. With respect to fatigue cracking, the most significant factor is the temperature differential or thermal gradient between the top and the bottom of the slab and the moisture in the slab. The thermal gradient can be either positive (i.e., the top of the slab is warmer than the bottom, or negative, with the top of the slab cooler than the bottom). A positive thermal gradient causes the top to curl downward, which is resisted by the support. This creates restraint tensile stress at the bottom of the slab with the maximum stress level midway between the joints. A negative thermal gradient causes the corners of the slab to curl upward, and this is resisted by the weight of the slab. This results in tensile stress at the top of the corner region of the slab. The downward curling of the slab caused by the positive thermal gradient adds to the loading stress caused by the traffic. This can increase the critical stresses in the concrete slab dramatically, especially with large positive thermal gradients. The fatigue damage caused during the negative temperature gradients is negligible as the curling stresses subtract from the load stresses. Therefore, only the positive thermal gradients were considered in this study.

The temperature gradient in the pavement slabs change continuously through the day. The main factors affecting the magnitude of temperature gradients are air temperature, wind speed, and the amount of time the slabs are exposed to the sun. To adequately account for the effect of temperature gradients, hourly temperature gradient data for the entire year from the representative years were needed. The Climatic-Materials-Structural (CMS) pavement analysis program was used to generate the needed data from the monthly derived climatic data in the LTPP data base.[8] The CMS model has been validated and has been shown to predict temperatures in pavement slabs reasonably well. The CMS model calculates the thermal gradient with depth considering air temperature, radiation heating and cooling, convection, cloud cover, wind speed, and material properties. From the LTPP climatic data base, the variables used to calculate the thermal gradients using the CMS model are shown in table 5.

Examples of the histograms of temperature differential versus frequency of occurrence in percent time of the year for a few sections are given in figures 1 through 4. Average monthly maximum temperature and average monthly minimum temperature were available for most of the JPCP sections. However, only 56 sections out of a total of 129 sections in the GPS-3 experiment had percent sunshine data and only 81 sections had wind speed data. For the sections without either percent sunshine data or wind speed data, the average value of these parameters for other sections in the same State or the surrounding States were used instead.

Transverse Cracking Data

The manual transverse cracking data are stored in the table MON_DIS_JPCC_REV (file extension *.M08). The data elements used in the evaluation are TRANS_CRACK_NO_L, TRANS_CRACK_NO_M, and TRANS_CRACK_NO_H. The parameter of interest is the percent slabs cracked in the 152.4-m section, which can be calculated as:

Table 5. Data elements needed for the CMS model and the corresponding LTPP tables.

Data Element	LTPP Table Name	File Extension
Average monthly maximum temperature (1959 to 1989)	ENV_MONTHLY_PARAMETER	*.E03
Average monthly minimum temperature (1959 to 1989)		
Average monthly wind speed (1959 to 1989)		
Average monthly percent sunshine (1959 to 1989)		
PCC slab thickness	TST_PC06 INV_LAYER	*.T2 *.I03
Latitude	INV_ID	*.I00

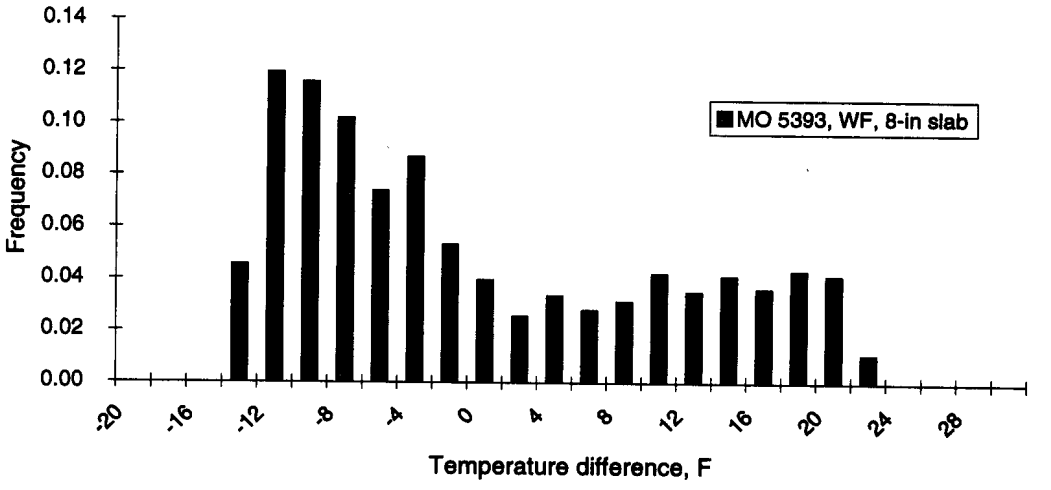

(1 °F = 0.56°C, 1 in = 25.4 mm)

Figure 1. An example of temperature difference distribution of a wet-freeze section for an average year.

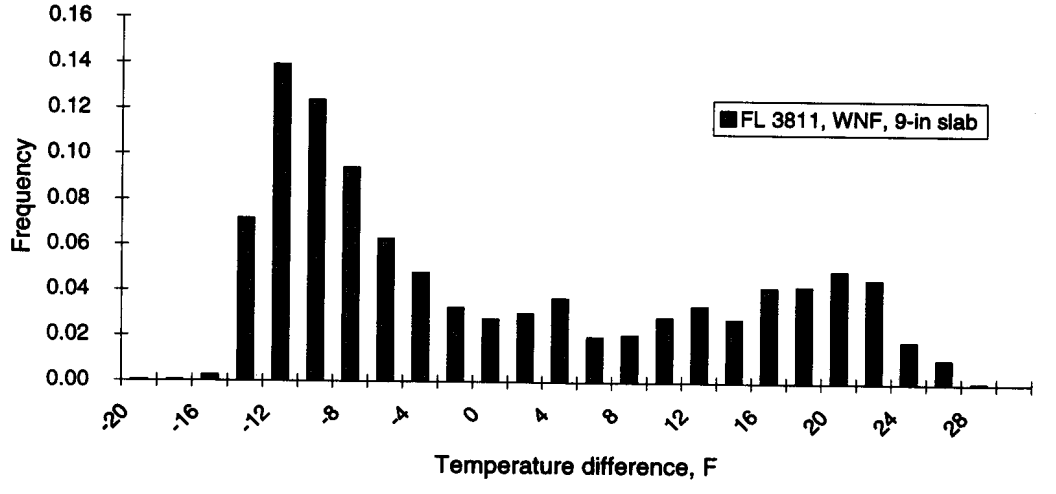

(1 °F = 0.56°C, 1 in = 25.4 mm)

Figure 2. An example of temperature difference distribution of a wet no-freeze section for an average year.

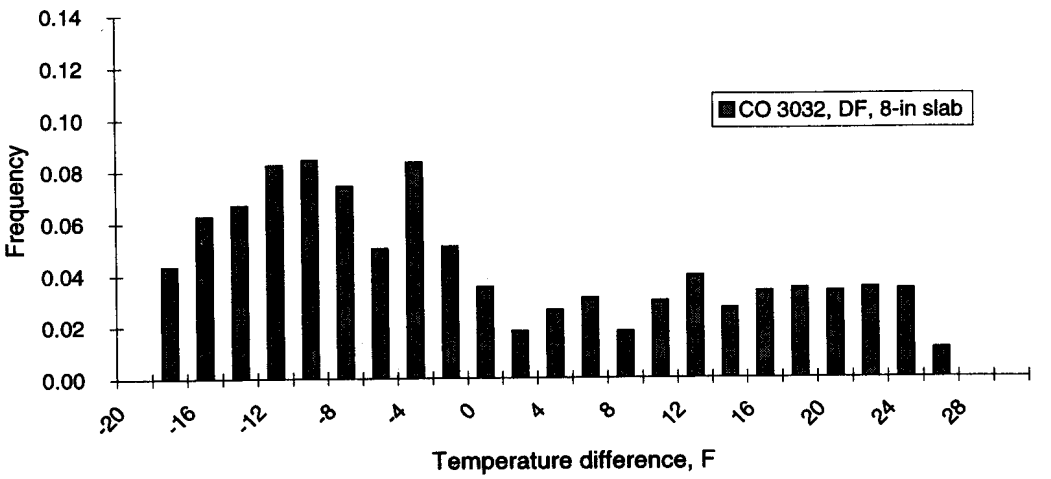

(1 °F = 0.56 °C, 1 in = 25.4 mm)

Figure 3. An example of temperature difference distribution of a dry-freeze section for an average year.

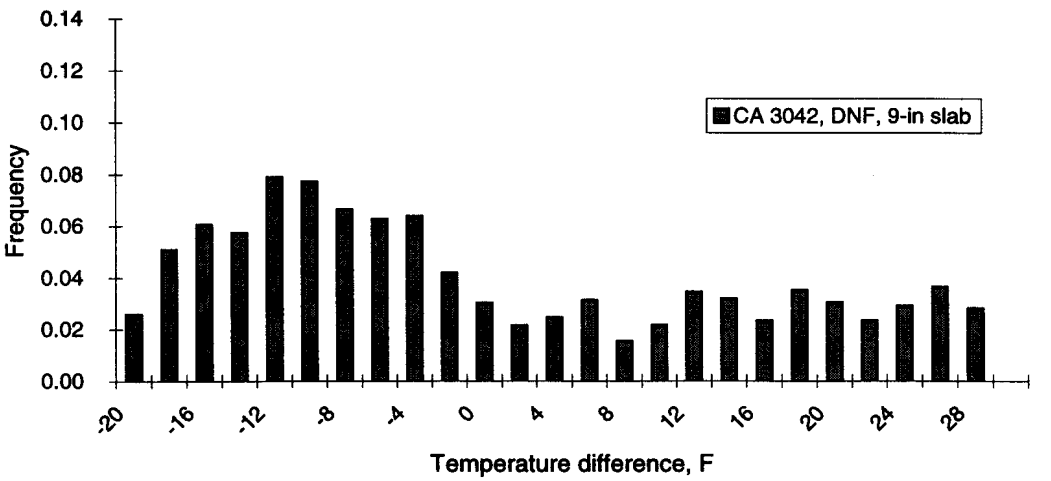

(1 °F = 0.56 °C, 1 in = 25.4 mm)

Figure 4. An example of temperature difference distribution of a dry no-freeze section for an average year.

$$\%\ slabs\ cracked = (Total\ TRANS\_CRACKED\_NO) * \frac{average\ joint\ spacing,\ m}{152.4} \quad \textbf{(10)}$$

where: *TOTAL TRANS_CRACK_NO* = TRANS_CRACK_NO_L + TRANS_CRACK_NO_M + TRANS_CRACK_NO_H.

For the sections with traffic data but no manual transverse cracking data, the photographic distress data in the table MON_DIS_PADIAS_JC (file extension *.M17) were used. No attempt was made to differentiate between midslab and non-midslab transverse cracking or random cracking (construction related) as these data were not readily available. It was assumed that a very low amount, if any, of random cracking was present in the GPS-3 sections.

Joint Faulting Data

The joint faulting data were derived from the table MON_DIS_JPCC_FAULT (file extension *.M09). The table lists the values for joint faulting at the corner and at the wheelpath at each joint. The values used in the analysis were the corner values, averaged along the 152.4-m length of the section.

Sections with Missing Data

The total number of GPS-3 sections is 129 and the total number of GPS-4 sections is 68. Only GPS-3 sections were used for the analysis of fatigue cracking. For joint faulting analysis, both GPS-3 and GPS-4 were used. However, as discussed, many sections were missing key data such as traffic and distress data. These sections were not used in the analysis. For analysis of fatigue cracking, data from 52 sections (with traffic data availability) were used. For the analysis of faulting data, data from 57 sections (20 with aggregate interlock joints and 37 with doweled joints) were used.

It should be clear from the information presented in this chapter that LTPP test sections have zero utility if any of the critical data elements are missing or are of questionable quality.

CHAPTER 3 - FATIGUE CRACKING ANALYSIS

Introduction

Transverse fatigue cracking is one of the most important distress measures that affects the pavement performance for JPCP. This occurs as a result of repeated application of high stresses in the concrete slabs that induces fatigue failure. The high stress levels are caused by the combined effects of the shrinkage of the concrete slab, thermal curling, moisture warping, and traffic loading. Fatigue cracking is caused by the repeated application of traffic and environmental loadings at stress levels lower than the failure stress level. This section documents the mechanistic evaluation of the fatigue cracking that occurred in LTPP JPCP sections.

The keys to the evaluation of the transverse fatigue cracking in JPCP include the following:

- Reliable determination of the stresses at the critical location under both traffic loading and the environmental effects; and
- Accurate prediction of the fatigue damage using a reliable fatigue damage model.

Stress Calculation

In this study, the fatigue analysis was conducted assuming that the transverse cracks observed in JPCP are the result of fatigue failure initiated at the slab bottom near the mid-slab locations. Therefore, for normal 3.66-m-wide sections, the critical damage location is at the bottom of the longitudinal edge, halfway between the two transverse joints that border the slab. The maximum wheel-load stress occurs at the longitudinal edge when the load is placed right along the edge. The stresses resulting from slab temperature curling also add significantly to the load stresses when the slabs are exposed to high positive temperature gradients. Combined, the magnitude of stresses at the longitudinal edge is so much greater than the stresses at any other location that fatigue cracking in JPCP is controlled by the few axle loads that pass along or near the slab edge while the slab is subjected to a large positive temperature gradient.

There are many procedures to calculate the stresses induced in the concrete slab. Finite element analysis technique is the most accurate technique for the calculation of slab stresses. In the NCHRP 1-26 study, a procedure was developed to determine the structural responses that can consider different pavement conditions and different loading conditions based on the plate on liquid [Winkler foundation model (the Westergaard model)].[9] The stresses calculated from the Westergaard model are modified using results from the finite element model, ILLI-SLAB, to make the necessary adjustments for joint spacing, load transfer, load location, load configuration, slab curl, etc.[10,11,12] All these modifications were validated using factorial matrixes of the key variables.[9] This approach was selected in this study to calculate the critical tensile stresses in the concrete slab.

Load Stress

The NCHRP 1-26 equations start with Westergaard's "new" formula for edge loading for a circular load.[13] This approach is based on medium-thick plate theory on a dense liquid foundation. The closed form solution for the edge load stress, σ_e, is given below:

$$\sigma_e = \frac{3(1+\mu)P}{\pi(3+\mu)h^2}\left[\ln\frac{Eh^3}{100ka^4} + 1.84 - \frac{4\mu}{3} + \frac{1-\mu}{2} + 1.18(1+2\mu)\frac{a}{\ell}\right] \quad \textbf{(11)}$$

where: P = Total applied load, lbf.
μ = Poisson's ratio.
E = Modulus of elasticity of PCC, lbf/in^2.
h = Slab thickness, in.
k = Modulus of subgrade reaction, lbf/in^2/in.
a = Radius of the applied load, in.
ℓ = Radius of relative stiffness, in, defined as follows:.

$$\ell = \left[\frac{Eh^3}{12(1-\mu^2)k}\right]^{0.25} \quad \textbf{(12)}$$

where: E = Modulus of elasticity of PCC, lbf/in^2.
h = Slab thickness, in.
μ = Poisson's ratio.
k = Modulus of subgrade reaction, lbf/in^2/in.

(Note: 1 lbf = 4.448 kN, 1 lbf/in^2 = 0.895 kPa, 1 in = 25.4 mm, lbf/in^2/in = 0.27 MPa/m)

The load stresses are determined by applying various adjustment factors to the edge stress calculated using Westergaard's equation (equation 1). The adjustments are made for the slab size effect, widened lane, tied concrete shoulder, and stabilized base. Regression equations are available for determining each of these factors. The final load stress is computed as follows:

$$\sigma_{load} = f_{Slab} * f_{Base} * f_{WL} * f_{Tied} * \sigma_e \quad \textbf{(13)}$$

where: σ_{load} = Load stress, lbf/in^2.
f_{Slab}, f_{Base}, f_{WL}, f_{Tied} = Adjustment factors for slab size, stabilized base, widened lane, and tied concrete shoulder.
σ_e = Stress obtained using Westergaard's edge load equation for circular loads, lbf/in^2.

The equivalent single-axle radius (ESAR) concept is used to handle multiple wheel loads, and adjustments are made to account for the slab size effect, widened traffic lane, tied concrete shoulder, and the presence of a stabilized base.

Equivalent Single-Axle Radius

The ESAR is the equivalent single wheel radius for a multiple wheel load that will produce the same stress intensity as the single circular wheel load having a radius of loaded area equal to ESAR at the critical location. The application of the ESAR concept allows the use of a closed form solution to determine the maximum stress under a multiple wheel load. The axle configurations analyzed in this study are shown in figure 5.

The equivalent single-axle radius for the dual wheel load is obtained using the following equation:[9]

$$\frac{a_{eq}}{a} = 0.909 + 0.339485\frac{S}{a} + 0.103946\frac{a}{\ell} - 0.017881\left(\frac{S}{a}\right)^2 - 0.045229\left(\frac{S}{a}\right)^2\frac{a}{\ell} + 0.000436\left(\frac{S}{a}\right)^3 - 0.301805\frac{S}{a}\left(\frac{a}{\ell}\right)^3 + 0.034664\left(\frac{S}{\ell}\right)^2 + 0.001\left(\frac{S}{a}\right)^3\frac{a}{\ell} \quad (14)$$

$$\textit{Limits:} \quad 0 \le (S/a) \le 20, \quad 0 \le (a/\ell) \le 0.5$$

where: a_{eq} = Equivalent single axle radius of dual wheels.
a = Radius of the applied load.
S = Dual wheel spacing.
ℓ = Radius of relative stiffness.

The equivalent single-axle radius for the dual wheel tandem axle load is given by the following equation:[9]

$$\frac{a_{eq}}{a} = 2.199479 + 0.74761\left[ln\left(\frac{t}{a}\right)ln\left(\frac{a}{l}\right)\right] + 0.548071\left[ln^2\left(\frac{t}{a}\right)\right] - 0.486597\left[ln^2\left(\frac{t}{a}\right)\right]\left[ln\left(\frac{a}{l}\right)\right] - 0.29507\left[ln^3\left(\frac{t}{a}\right)\right] - 0.028116\left[ln^3\left(\frac{a}{l}\right)\right] \quad (15)$$

$$\textit{Limits:} \quad 4 < (t/a) < 16, \quad 0.05 < (a/l) < 0.5$$

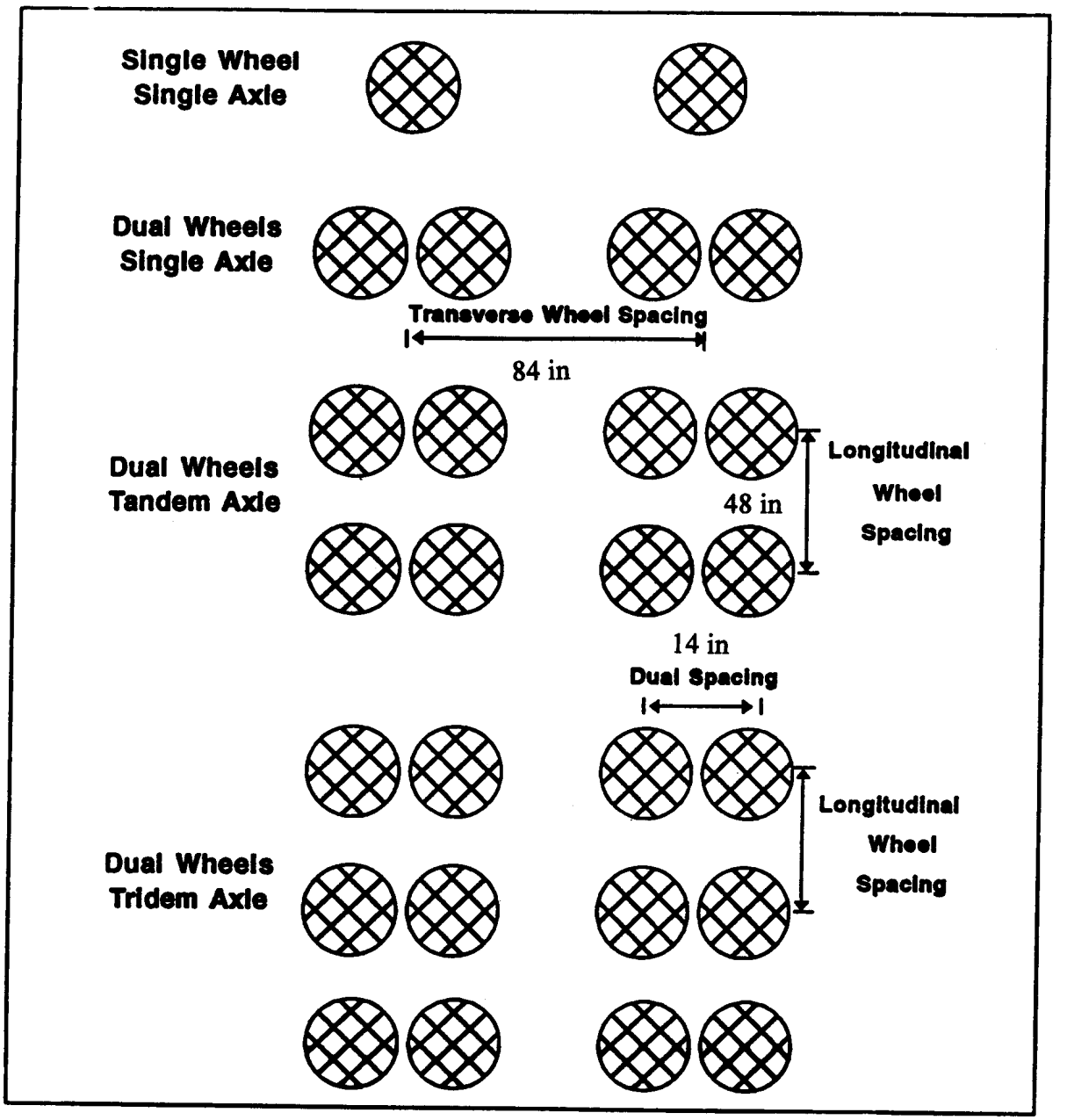

(1 in = 25.4 mm)

Figure 5. Axle configurations analyzed.

where: t = Distance between wheels parallel to the pavement edge, in.

(Note: 1 in = 25.4 mm)

The regression equation for the equivalent single-axle radius for the dual wheel tridem axle load is given by the following equation:[9]

$$\frac{a_{eq}}{a} = 1.542864 + 0.567442\left(\frac{t}{a}\right) + 5.465697\left(\frac{a}{l}\right) + 17.371416\left(\frac{a}{l}\right)^2 - 0.704714\left(\frac{S}{l}\right) - 2.61563\left(\frac{t}{l}\right) + 0.087538\left(\frac{t}{a}\right)\left(\frac{S}{a}\right) - 0.000359\left(\frac{t}{a}\right)\left(\frac{S}{a}\right)^2 \quad \textbf{(16)}$$

Limits: $3 \le (S/a) \le 15$
$4 \le (t/a) \le 10$
$0.05 \le (a/l) \le 0.3$

where: t = Distance between wheels parallel to the pavement edge.

Slab Size Effect

Edge stress calculated by the Westergaard solution is for slabs of infinite size. Ioannides et al. introduced a normalized length term, *L/l,* to correct the Westergaard edge stresses for slab size.[14] In the NCHRP 1-26 study, a factorial was designed for the key variables affecting the stress, and a regression equation was developed to account for the finite slab size, as shown below:[9]

$$\frac{\sigma_{ill}}{\sigma_{\infty}} = 0.582282 - 0.533078\left(\frac{a}{l}\right) + 0.181706\left(\frac{L}{l}\right) - 0.019824\left(\frac{L}{l}\right)^2 + 0.109051\left(\frac{a}{l}\right)\left(\frac{L}{l}\right) \quad \textbf{(17)}$$

Limits: $3 \le (L/l) \le 5$
$0.05 \le (a/l) \le 0.3$

where: σ_{ill} = ILLI-SLAB edge stress for finite slab.
σ_{∞} = Westergaard edge stress for infinite slab.
l = Radius of relative stiffness.
L = Slab length.

Tied Concrete Shoulder

The following two equations were developed in NCHRP 1-26 to correct for the effect of a tied shoulder:[9]

$$\frac{\sigma_{AGG}}{\sigma_{AGG=0}} = 0.99864 - 0.51237\left(\frac{a}{l}\right) - 0.0762\left[ln\left(\frac{AGG}{kl}\right)\right] + 0.00315\left[ln^2\left(\frac{AGG}{kl}\right)\right] + 0.015936\left[\left(\frac{a}{l}\right)^2 ln^2\left(\frac{AGG}{kl}\right)\right] \quad \textbf{(18)}$$

Limits: $5 \le (AGG/kl) \le 50000$
$0.05 \le (a/l) \le 0.3$
and

$$\frac{\sigma_{AGG}}{\sigma_{AGG=0}} = 1 - 0.025169\left(\frac{AGG}{kl}\right) - 0.086034\left(\frac{a}{l}\right)\left(\frac{AGG}{kl}\right) \quad \textbf{(19)}$$

Limits: $0 \le (AGG/kl) \le 5$
$0.05 \le (a/l) \le 0.3$

where: AGG = Aggregate-interlock factor.
σ_{AGG} = Edge bending stress with aggregate interlock at AGG/kl.
σ_{AGG-0} = Free edge bending stress.

Stabilized Base

When base layer is a stabilized material with an elastic modulus comparable to the elastic modulus of concrete slab ($E_{Base}/E_{Slab} > 0.1$), then the base layer can have a significant effect on the slab response to load. Two cases were considered in the NCHRP 1-26 study, namely a bonded or unbonded base. The following regression equation was developed to correct the effect of an unbonded base:[9]

$$\frac{\sigma_{ill}}{\sigma_{west}} = 0.0477629 + 0.265264\left(\frac{a}{l}\right) + 0.953195\left(\frac{h_{efft}}{h_1}\right)^{-2} - 0.26083\left(\frac{a}{l}\right)\left(\frac{h_{efft}}{h_1}\right)^{-2} \quad \textbf{(20)}$$

Limits: $1 \le (h_{eff}/h_1)2 \le 1.6$
$0.05 < (a/l) < 0.3$

where: σ_{ill} = ILLI-SLAB edge stress with a base.
σ_{west} = Westergaard edge stress without a base.
h_{effi} = Effective thickness.

$$h_{eff} = \sqrt{h_1^2 + h_2^2 \frac{E_2 h_2}{E_1 h_1}}$$

h_1 = Slab thickness.
h_2 = Base thickness.

For the bonded base case, an equivalent layer can be calculated based on the transformed section concept. The following equations can be used to calculate the effective slab thickness:

$$h_{1f} = \sqrt[3]{\left(h_1^3 + 12 h_1 \beta^2\right)} \tag{21}$$

$$h_{2f} = \sqrt[3]{\left(h_2^3 + 12 h_2 \alpha^2\right)} \tag{22}$$

where:

$$\alpha = \frac{\left(\frac{1}{2}\right) h_1 (h_1 + h_2)}{h_1 + h_2\left(\frac{E_1}{E_2}\right)} \tag{23}$$

$$\beta = \left(\frac{1}{2}\right)(h_1 + h_2) - \alpha \tag{24}$$

h_{1f} = Transformed slab thickness.
h_{2f} = Transformed base thickness.
h_1 = Slab thickness.
h_2 = Base thickness.

Widened Outer Lane

On widened lane sections, the critical location for fatigue damage is the bottom of the slab, directly under the wheel path and at the midslab location. Studies have shown that the slabs are almost never loaded at the outer edge on widened lane sections.[7] Therefore, the following

adjustment factor was used to obtain the maximum stress directly under the wheel load for the few cases of widened lanes:[9]

$$f_{WL} = 0.454147 + \frac{0.013211}{D/\ell} + 0.386201\frac{a}{D} - 0.24565\left(\frac{a}{D}\right)^2 + 0.053891\left(\frac{a}{D}\right)^3 \quad (25)$$

where: f_{WL} = Adjustment factor for widened lane.
= 1.0 if standard-width lane of 3.66 m.
a = Radius of loaded area.
D = Mean wheel location, in from outer edge.
ℓ = Radius of relative stiffness.

Curling Stress

The curling stress is determined using the following equation and then combined with the load stress using a regression coefficient in the NCHRP 1-26 procedure:

$$\sigma_c = \frac{C\ E\ \alpha_T\ \Delta T}{2} \quad (26)$$

where: σ_c = Curling stress.
C = Curling stress coefficient.
E = Concrete modulus of elasticity.
α_T = Concrete coefficient of thermal expansion.
ΔT = Temperature difference between the top and bottom of the slab.

This equation was developed by Westergaard, and Bradbury developed the coefficients for solving this equation.[15,16] For maximum stress at the longitudinal edge, the curling stress coefficient is given by the following equation:

$$C = 1 - \frac{2\cos\lambda\cosh\lambda}{2\sin\lambda\sinh\lambda}(\tan\lambda + \tanh\lambda) \quad (27)$$

$$\lambda = \frac{L}{\ell\sqrt{8}} \quad (28)$$

where: L = Slab length.
ℓ = Radius of relative stiffness.

Warping Stresses

Warping is the result of non-uniform shrinkage between the top and bottom of the slab. The top of the slab is usually drier than the bottom throughout the year. Therefore, moisture gradient generally tends to cause lifting of the slab corner or warping. The warping is resisted by the slab weight, causing warping restraint stresses in the slab. The moisture gradients could be treated as equivalent temperature gradients, but insufficient research is available to adequately quantify this effect.

During initial construction, as concrete dries it will shrink in volume and thus cause upward warping and warping stresses. The shrinkage normally occurs during concrete's initial curing phase, and before it has attained its full strength. Since the shrinkage warping stresses occur early in the concrete aging cycle, and the stresses are long term, some of the warping stresses may be relieved by concrete creep. Again, there is not enough information to quantify the effect. Therefore, the warping stresses are not considered in this evaluation. It was assumed that the warping effects are indirectly accounted for during the calibration/validation of the procedure.

Combined Stress

The combined stress due to load and curling is obtained using the following equation:

$$\sigma_{combined} = \sigma_{load} + R * \sigma_{curl} \tag{29}$$

where: $\sigma_{combined}$ = Combined edge stress.
σ_{load} = Load stress.
R = Regression coefficient.
σ_{curl} = Curling stress.

The regression coefficient R is determined using the following equation:[9]

$$R = 1.062 - 0.015757\,dT - 0.0000876\,k - 1.068\frac{L}{\ell} + 0.387317\,dT\frac{L}{\ell} + 1.17x10^{-11}E\,dTk - 1.81x10^{-12}E\,dT^2k - 1.051x10^{-9}E\left(\frac{L}{\ell}\right)^2 kdT + 1.84x10^{-11}E\,dT^2\frac{L}{\ell}k - 1.7487\left(\frac{L}{\ell}\right)^2 dT + 0.000034351\,dT^3 + 86.97\left(\frac{L}{\ell}\right)^3 - 0.00816396\,dT^2\frac{L}{\ell} \tag{30}$$

where: dT = $\alpha\Delta T \times 10^5$.
α = Concrete coefficient of thermal expansion, ϵ/°F.

ΔT = Temperature difference through the slab, °F.
k = Subgrade modulus of reaction, lbf/in^2/in.
L = Slab length, in.
ℓ = Radius of relative stiffness, in (equation 11).
E = Concrete modulus of elasticity, lbf/in^2.

(Note: 1ϵ/°F = 1.8ϵ/°C, 1 °F = 0.56°C, 1lbf/in^2/in = 0.27 MPa/m, 1 in = 25.4 mm, 1 lbf/in^2 = 6.895 kPa)

The coefficient R is needed because the load and curling stresses are not directly additive. Curling causes various parts of the slab to lift off of the base, invalidating the full contact assumption made in the load stress calculation. The regression coefficient R provides the necessary adjustment to the curling stress to give the correct combined stress.

Structural Model

Several fatigue models are available to calculate the total number of a specific load coverages to failure.[3,9] The fatigue model developed in the NCHRP 1-26 study was used in this project. The model, which gives the mean number of coverages to failure, defined as 50 percent slabs cracked, is of the following form:

$$LogN = -1.7136R + 4.284 \text{ for } R > 1.25$$
$$LogN = 2.8127R^{-1.2214} \text{ for } R < 1.25 \quad (31)$$

where: R = Ratio of flexural stress, due to load and climatic factors, to the mean modulus of rupture of the concrete.
N = Number of coverages to 50 percent slabs cracked.

Fatigue Damage Calculation

The fatigue damage was determined using Miner's hypothesis, which can be formulated as:

$$FD = \sum \frac{n_{ijk}}{N_{ijk}} \quad (32)$$

where: FD = Total fatigue damage at the critical location in the slab.
n_{ijk} = Number of load repetitions of i^{th} axle group, j^{th} load level, and k^{th} temperature gradient.
N_{ijk} = Number of allowable load repetitions of i^{th} axle group, j^{th} load level, and k^{th} temperature gradient.
i = A counter for axle group (single dual, tandem dual, and tridem dual).

j = A counter for axle load magnitude, total of 83 axle load levels in the LTPP data base for the single, tandem, and tridem axles.

k = A counter for temperature gradient levels, total of 15 levels used.

The number of load repetitions, n_{ijk}, was computed using traffic data from the LTPP traffic data base for different axle load group and load magnitude. It was corrected for the truck lateral distribution. Temperature gradient was represented by the frequency of the different temperature difference happenings in a typical year, as discussed previously. Therefore, the number of load repetitions of a specific axle load group and load level, for a specific temperature gradient level, can be formulated as follows:

$$n_{ijk} = n_{ij} * Dist * Freq\text{-}T \quad (33)$$

where: n_{ij} = Load repetition count from the LTPP data base for a specific load group and magnitude.

Dist = Lateral truck distribution factor for loads within 6 in from the edge (8 percent).

Freq-T = Frequency of a specific temperature gradient happening in a typical year.

A spreadsheet was developed to calculate the allowable number of load repetitions for each axle load group at each load level for a specific temperature gradient. This was then used with the actual load repetition in each group to calculate the total fatigue damage. The calculated load and curling stresses were compared with the results from the computer program ILLI-CONC developed under the NCHRP 1-26 project to ensure the correctness of the spreadsheet. It is worth noting that, since there were 83 total load levels and 15 temperature gradient levels used for the fatigue damage calculation, a total of 1,245 calculations for each LTPP section was needed to obtain the cumulative fatigue damage.

Correlation Between GPS-3 Fatigue Cracking and the Calculated Fatigued Damage

At the time of the analysis, a total of 52 JPCP (GPS-3) sections had at least 1 year of traffic monitoring data. Only these 52 sections were used in the analysis. The specific data used in the analysis for these 52 sections are given in appendix A. The fatigue analysis results of the 52 GPS-3 test sections are shown in figure 6. Also shown in the graph is a transverse cracking model recently developed as part of a completed FHWA concrete pavement performance study.[17] This model is based on field observations from 303 in-service concrete pavements in the United States and Canada in 1987 and 1992. A total of 465 data points were used to develop the model. The model is listed below:

$$percent\ cracking = \frac{100}{1 + 1.41FD^{1.66}} \quad (34)$$

As shown in figure 6, there were only 15 sections with traffic data in GPS-3 showing some form of transverse cracking. The sections with fatigue cracking generally follow the trend of the model except for a couple of outliers. There also are many sections with large theoretically calculated fatigue damage values but with no transverse cracking present, indicating that the fatigue damage procedure used and/or the input data used do not fully simulate the fatigue cracking process in JPCP.

Sensitivity Analysis

This section is concerned with the sensitivity of the fatigue damage calculation as a function of some key data elements such as traffic counts, modulus of rupture of the concrete, concrete elastic modulus, concrete thermal expansion coefficient, and subgrade modulus of reaction. A Missouri section, SHRP ID of 5393, was selected to conduct the sensitivity analysis. The following results are all based on the data from this pavement section.

Traffic counts represent the loading conditions of the pavement over time. The availability and accuracy of the traffic spectrum data are always a great concern in the mechanistic evaluation of the pavement distresses. When Miner's hypothesis is used to calculate the cumulative fatigue damage as given in equation 20, the total cumulative fatigue damage is the linear combination of the traffic counts divided by the allowable number of repetitions under the specific condition. Figure 7 shows the variation of the cumulative fatigue damage when the traffic counts are all doubled or halved uniformly for all load configuration and load levels.

Modulus of rupture of the concrete is another very important variable in the mechanistic evaluation. Figure 8 gives the sensitivity plot of the fatigue damage with the variation of the modulus of rupture of the concrete. As shown, small changes in *Mr* will significantly affect the final calculated fatigue damage. Similarly, as shown in figure 9, variation in the elastic modulus value will have a significant effect on the calculated fatigue damage. The sensitivity plot of the PCC thermal expansion coefficient (figure 10) also shows a significant effect on the calculated fatigue damage.

Figures 11 and 12 show the fatigue damage as a function of concrete Poisson's ratio and the subgrade k-value. As shown, within the range of values commonly used, fatigue damage computation is not dependent on either Poisson's ratio or modulus of subgrade reaction used.

Summary

Analysis of the LTPP fatigue cracking data indicates that the LTPP data have a high potential for supporting the development of M-E procedures for the prediction of fatigue cracking. The analysis presented was limited to showing the potential for use of the LTPP data for calibrating/validating existing M-E procedures. No specific calibration of the NCHRP 1-26 model/procedure for prediction of fatigue cracking was attempted because it was considered premature to do so at this time, for the following reasons:

1. Limited number of test sections exhibiting higher levels of fatigue cracking.

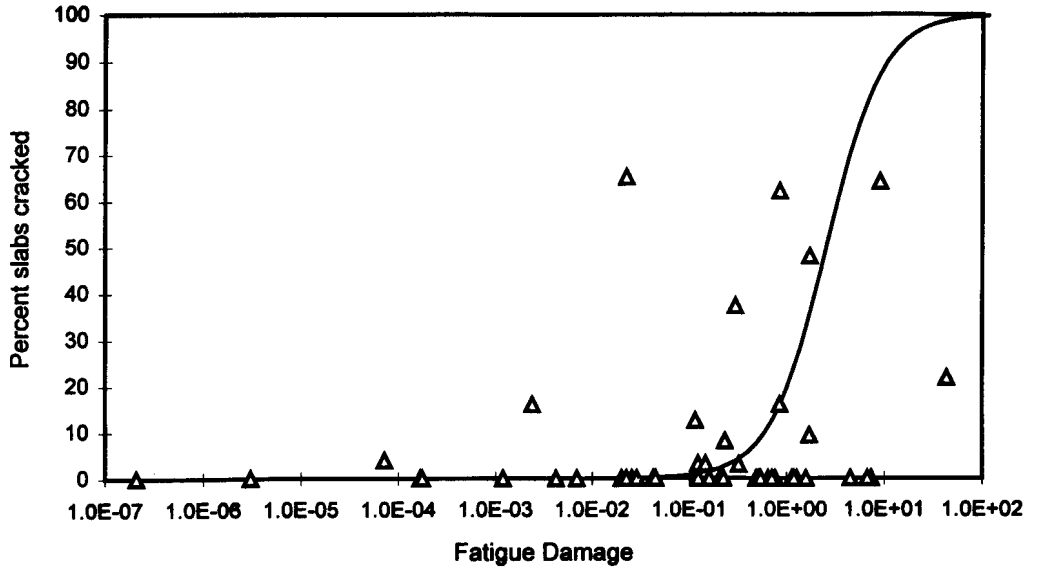

Figure 6. Fatigue analysis results of LTPP GPS-3 data.

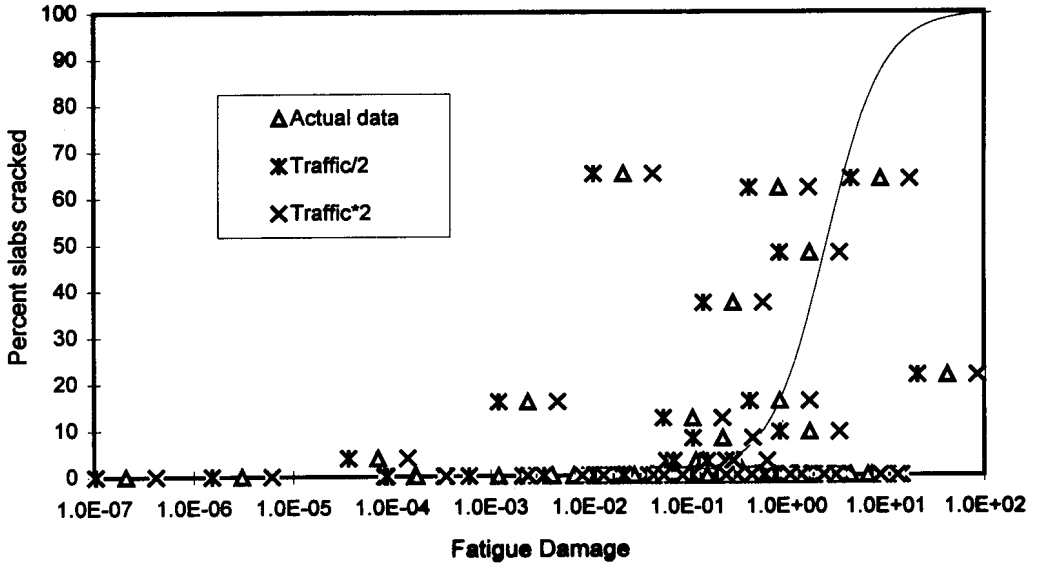

Figure 7. Sensitivity of the cumulative fatigue with traffic counts.

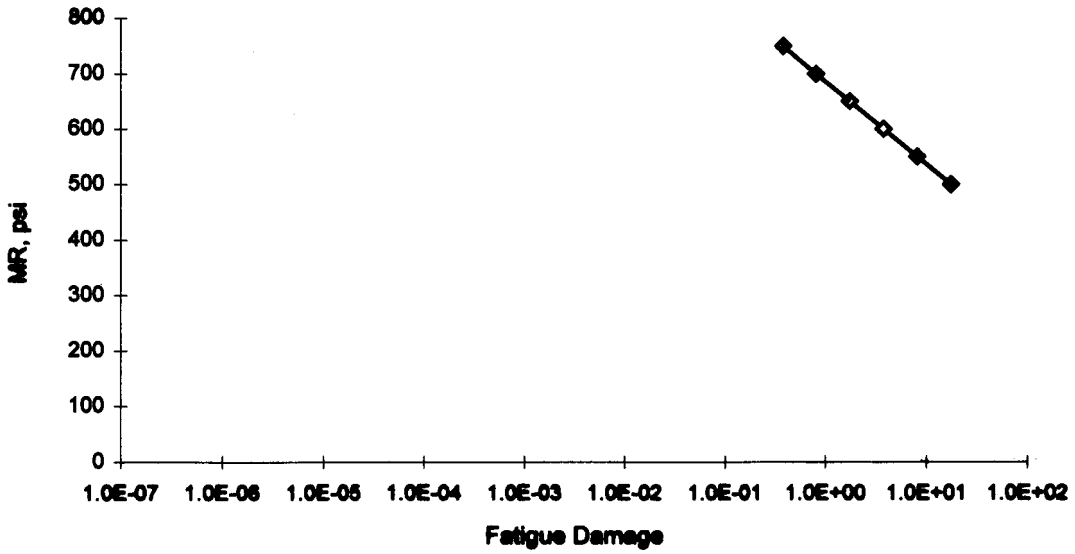

(1 psi = 6.895 kPa)

Figure 8. Sensitivity plot of the fatigue damage with change of modulus of rupture.

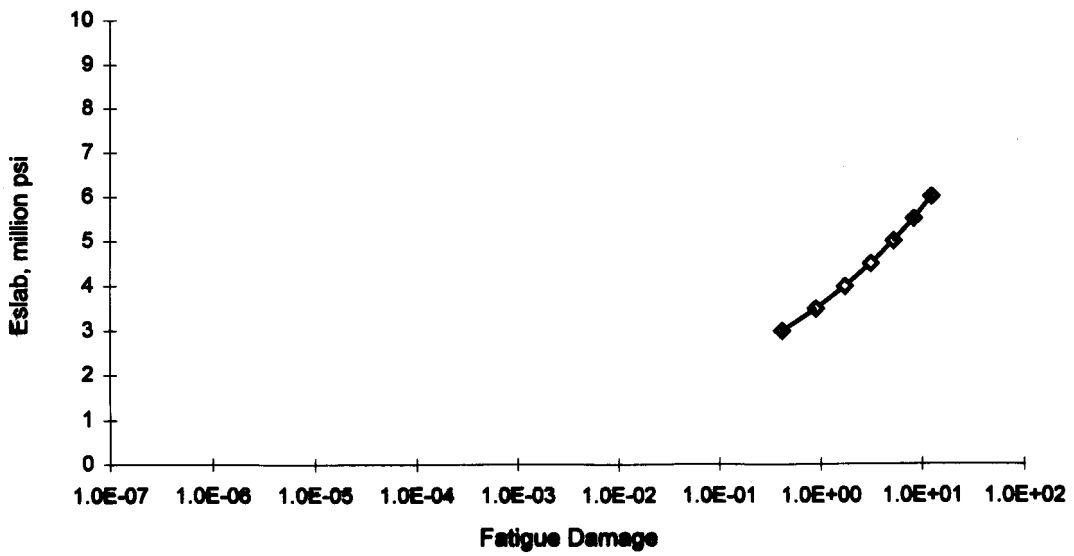

(1 psi = 6.895 kPa)

Figure 9. Sensitivity plot of the fatigue damage with change of elastic modulus of the slab.

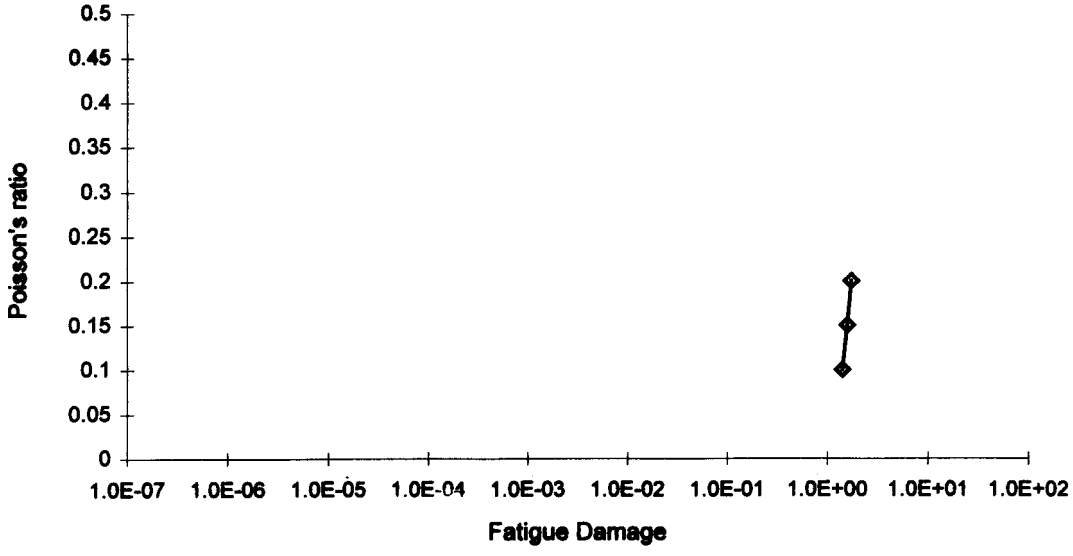

(1°F = 0.56°C)

Figure 10. Sensitivity plot of the fatigue damage with change of the PCC thermal expansion coefficient.

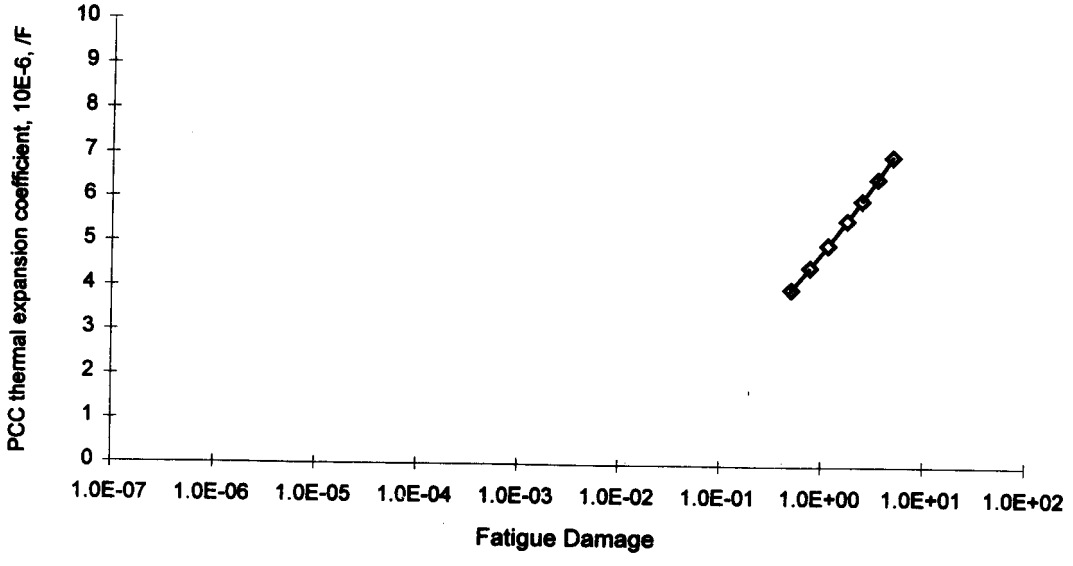

Figure 11. Sensitivity plot of the fatigue damage with change of Poisson's ratio of the slab.

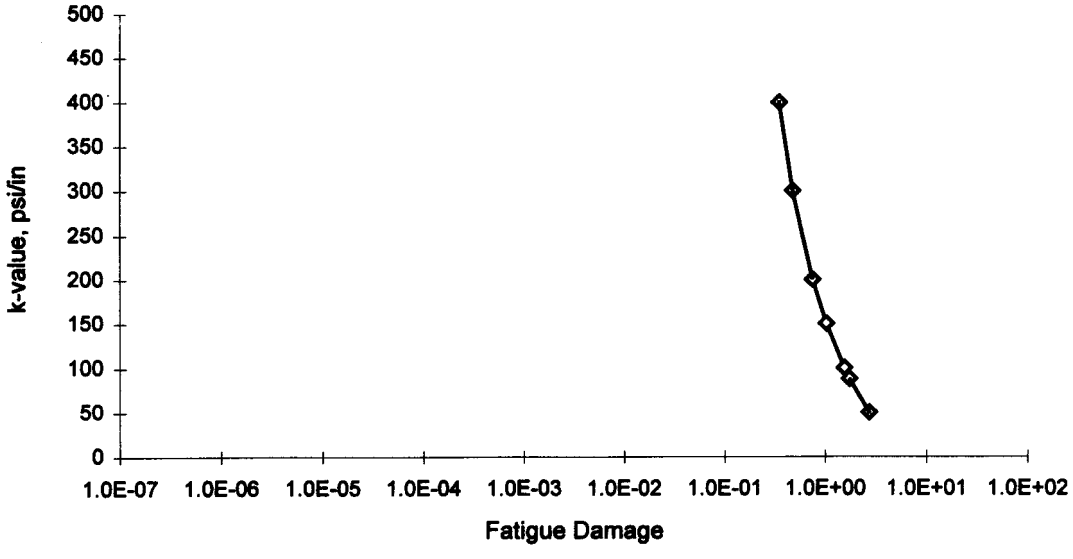

(1 psi/in = 0.27 MPa/m)

Figure 12. Sensitivity plot of the fatigue damage with change of subgrade k-value.

2. Concern with the quality of the extrapolated traffic data. Even though weigh-in-motion data are beginning to be available for many GPS test sections, the sampling precision, the reliability of the axle load measurements, lateral distribution of traffic, and the backcasting of traffic need further clarity.

3. Concern with the fatigue cracking distress data. The fatigue data need to be re-evaluated to ensure that random cracking data are omitted from the fatigue cracking data.

4. A practical procedure needs to be developed to incorporate seasonal effects.

5. A better characterization needs to be developed to incorporate curling and warping effects. The availability of site specific coefficient of thermal expansion for the concrete would greatly aid in this effort.

In summary, it is concluded that the NCHRP 1-26 approach for predicting fatigue cracking (in terms of pertinent slabs cracked) appears to be reasonable, given the many unknowns that continue to hinder a complete development of the prediction methodology. As the LTPP data base is progressively improved upon, both in terms of quality and in terms of data coverage, it is expected that the NCHRP 1-26 approach will be improved and that a more reliable and better calibrated fatigue cracking prediction procedure will be developed.

CHAPTER 4 - JOINT FAULTING ANALYSIS

Introduction

Transverse joint faulting is the difference in elevation of two adjacent slabs at a joint. Typically, the leave slab is at a lower elevation than the approach slab. Many jointed PCC pavements experience serious faulting with time. A faulting level in excess of 6 mm is considered unacceptable for high-volume highways. Faulting is significantly affected by the presence of dowel bars and permeable/non-erodible base, joint spacing, and subdrainage conditions.

Over the years, many studies have been conducted to research the development of faulting. Various models have been developed to predict faulting. Typically, these models have been empirical in form and incorporate the use of the equivalent single-axle load parameter to represent the traffic loading. The only mechanistic-based faulting prediction procedures are those developed under the sponsorship of the Portland Cement Association (PCA). These mechanistic-based models were the ones used in the analysis of the LTPP faulting data, as reported here.

The development of the PCA faulting models is described next.

Background

Prior to 1984, mechanistic thickness design procedures for concrete pavements were based on the principle of limiting the flexural stresses in a slab to avoid flexural fatigue cracks due to load repetitions. Erosion criteria were incorporated into the 1984 PCA design procedure since some modes of pavement distress, such as pumping, faulting, and shoulder distress, are unrelated to fatigue. Distress due to erosion is considered to be more closely related to slab deflections than to flexural stresses. At slab corners and edges in the presence of water and many repetitions of heavy axle loads, pumping (erosion of subgrade, subbase, and shoulder materials), voids under and adjacent to the slab, and faulting of pavement joints (especially in pavements at nondoweled joints) can occur. Voids or the loss of uniform support increase slab stresses and strains and can lead to premature cracking.

Attempts to correlate corner deflections to AASHO Road Test performance data, where all pavement sections were doweled, and to faulting studies were not successful.[18] The principal mode of failure at the AASHO Road Test was pumping of the granular subbase from under the slabs. It was found that, to be able to predict the AASHO Road Test performance, different values of deflection criteria would have to be applied to different slab thicknesses, and to a smaller extent, different slab support values.

Better performance prediction was obtained by correlation of the subbase pressure multiplied by the slab corner deflection. Subbase pressure at the slab-foundation interface is computed as the modulus of subgrade reaction, k, multiplied by the slab deflection. Power, or rate of work, with which an axle load deflects the slab is the parameter used for the erosion criterion. For a unit area, the power term incorporates the product of pressure and deflection

divided by a measure of the length of the deflection basin (radius of relative stiffness, ℓ). The concept is that a thinner pavement with its shorter deflection basin receives a faster punch than a thicker slab. At equal products of deflection and pressure, the thinner slab is subjected to a faster rate of work or power.

Successful correlation to AASHO Road Test performance data was developed in which the number of load repetitions, N, decreases with power, as defined in the following equation:[19]

$$P = \frac{p\ (unit\ area) * w * \dfrac{constant}{k^{0.0633}}}{\dfrac{l_e}{truckspeed}} \tag{37}$$

$$P = \frac{\dfrac{268.7 * p^2}{t}}{k^{0.73}} \tag{38}$$

where: P = Power (rate of work).
p = Pressure at slab-foundation interface, psi.
w = Corner deflection, in.
t = Slab thickness, in.
l_e = Radius of relative stiffness for elastic subgrade, in.
k = Modulus of subgrade reaction, pci.

(Note: 1 psi = 6.895 kPa, 1 in = 25.4 mm)

Truck speed is not a design variable but is used to introduce the length of deflection basin in time units. The selection of the elastic radius of relative stiffness for a Winkler subgrade and the addition of the modulus of subgrade reaction were arbitrarily selected to produce a single criteria that explained the performance of slabs with different thicknesses and foundation strengths at the AASHO Road Test.

Corner deflections (w) used in this model were computed based on a comprehensive finite element analysis of jointed concrete pavements.[19] In this analysis, corner deflections caused by applying a single axle load or a tandem axle load at the corner of concrete pavements with different parameters, such as concrete slab thickness, modulus of subgrade reaction, etc., were computed. Both doweled joints and aggregate-interlock joints were considered in the analysis. The effects of using tied concrete shoulder also was evaluated. From this comprehensive pavement analysis, equations were developed to compute corner deflections in the pavements when subjected to different axle loads. Essentially, corner deflections were expressed in terms of the radius of relative stiffness (ℓ) of the pavement system under consideration.

The development of the 1984 design erosion criteria was also generally related to studies on joint faulting. These studies included pavements in Wisconsin, Minnesota, North Dakota, Georgia, and California, and included a range of variables not found at the AASHO Road Test. Additional variables such as increased amounts of truck traffic, non-doweled pavements, a wider range of pavement service life, and stabilized subbases were included in the erosion criteria verification.

The analysis of data from the AASHO Road Test and available faulting studies resulted in the following erosion prediction equation:

$$\log N_i = 14.524 - 6.777 * \left(C_1 * P_i - 9.0\right)^{0.103} \quad \textbf{(39)}$$

where: N_i = Allowable load repetitions to end of design period for axle-group *i*.
P_i = Power term for axle-group *i*.
C_1 = $1 - (k / 2000 * 4 / t)^2$.

The constant C_1 is an adjustment factor that has a value close to 1.0 for normal granular subbases and decreases to approximately 0.90 for high-strength subbases.

The equation for erosion damage is:

$$EROSION, \% = 100 * \Sigma n_i * \left(\frac{C_2}{N_i}\right) \quad \textbf{(40)}$$

where: *EROSION* = Accumulated erosion, percent.
n_i = Expected number of axle-load repetitions for axle-group *i*.
N_i = Allowable number of repetitions for axle-group *i*.
C_2 = 0.06 for pavements without a shoulder and 0.94 for pavements with a tied concrete shoulder.

Truck wheel loads placed at the outside pavement edge create more severe deflection conditions than any other load position. As the truck placement moves inward a few millimeters from the edge, the effects decrease substantially. Only a small fraction of all the trucks run with their wheels placed at the edge. Studies on pavement edge encroachment show that most trucks are driven with the outside wheels placed about 0.6 m from the edge.[6,7] For the design procedure the most severe condition noted in encroachment studies of 6 percent of trucks at pavement edges was assumed. This added an additional factor of safety and accounted for recent changes in the United States permitting wider trailers. At increasing distances inward from the pavement edge, the frequency of load applications increases while the magnitude of stress and deflection decreases.

Where there is no tied concrete shoulder, corner loadings are critical. When a concrete shoulder is used, the greater number of loadings inward from the pavement corner are critical.

Most conventional analyses of concrete pavement systems assume that subbase-subgrade layers do not exist beyond the pavement edge. The MATS finite element computer program was used to investigate the effect and contribution of subbase-subgrade support away from the pavement edge.[20] For different moduli of subgrade reaction and slab thicknesses, the free corner deflections were equal to or less than 89.6 percent of those conditions without the outside subgrade-subbase support. The 10.4 percent corner deflection reduction factor was incorporated into the PCA erosion design charts for pavements without a tied concrete shoulder. For slabs with a concrete shoulder, the subgrade support outside the shoulder edge is too far from the truck traffic to have any beneficial effect on reducing deflections.

Development of Faulting Prediction Models Based on the Erosion Factor

During 1992, data from existing performance data bases were used to develop faulting prediction models to include the PCA erosion criteria as a parameter. Transverse joint data were collected from existing State Department of Transportation (DOT) pavement management data bases and pavement performance research data bases.[21,22,23] Joint faulting measurements obtained by the Construction Technology Laboratories also were added to the PCA data base.

The collection of faulting and traffic data used in the analysis is summarized by region and State in table 6. Survey data were collected in dry-freeze, dry non-freeze, wet-freeze, and wet non-freeze sections of the United States. Joint faulting data from a total of 509 projects were collected. Region classification criteria for wet or dry and non-freezing or freezing are summarized in table 7.[24]

The accumulated percent erosion was correlated with degree of faulting for each pavement section. Modulus of subgrade reaction (k-value) and increases in support due to granular and stabilized subbases were calculated using the PCA thickness design guideline procedures.[25] Truck load distribution and frequency were selected for each project from W-4 load tables. One-way average daily traffic (ADT) was used to estimate the proportion of trucks in the right lane. Erosion for several load categories was accumulated from the truck proportions, load frequency, and average daily truck traffic (ADTT).

Important environmental factors included in the analysis were the levels of moisture and temperature range. Levels of moisture were categorized by the freezing index (degree-days below 0°C), average annual precipitation, soil drainability (AASHTO soil type), and presence of longitudinal edge drains. Some previous research work has indicated that joint opening was statistically significant in predicting faulting only at non-doweled pavement joints. The degree of joint opening affecting joint load transfer and potential for faulting is a function of annual temperature range (maximum daily temperature minus minimum temperature), slab length (broadly categorized into jointed reinforced, JRCP, and jointed plain concrete pavement, JPCP), concrete coefficient of thermal expansion, and concrete drying shrinkage.

A statistical analysis computer program was used to develop the relationships between accumulated erosion and joint faulting. Non-linear regression analysis techniques were used in development of the faulting prediction model. An initial set of power parameters and variable

Table 6. Summary of States surveyed.

State	Climatic Region	No. of Projects	No. of Data Points	Data Source
Arizona	Dry Non-Freeze	7	7	ref. 22
California	Dry and Wet Non-Freeze	85	814	DOT, refs.21 & 22
Connecticut	Wet-Freeze	7	9	DOT
Florida	Wet Non-Freeze	50	283	DOT, refs. 22 & 23
Georgia	Wet Non-Freeze	28	65	ref. 21
Iowa	Dry and Wet Freeze	38	38	DOT
Illinois	Wet-Freeze, Wet Non-Freeze	8	15	DOT
Louisiana	Wet Non-Freeze	28	297	ref. 21
Michigan	Wet-Freeze	12	12	ref. 22
Minnesota	Dry-Freeze	105	921	DOT, refs.21 & 22
North Carolina	Wet Non-Freeze	13	63	DOT, ref. 22
New York	Wet-Freeze	21	21	refs. 22 & 23
Ohio	Wet-Freeze	59	59	refs. 22 & 23
Pennsylvania	Wet-Freeze	5	5	ref. 22
Utah	Dry-Freeze	33	231	ref. 21
Wisconsin	Dry and Wet Freeze	10	10	DOT
Total		509	2850	

Table 7. Climatic zone classification.

Climatic Zone	Annual Rainfall, in.	Freezing Index, F Degree-Days
Wet Non-Freeze	Greater than 28	Less than 100
Wet-Freeze	Greater than 28	Greater than 100
Dry Non-Freeze	Less than 28	Less than 100
Dry-Freeze	Less than 28	Greater than 100

(1 in = 25.4 mm, 1 F Degree-Day = 0.56 C Degree-Day)

coefficients were defined. A Taylor series expansion of the model was used near the initial set of parameters. Using partial derivatives with respect to each parameter and ignoring higher order terms, an approximation for the original function was derived that is linear in the power parameters and can then be solved with standard linear regression analysis techniques. This process was repeated until the sum of squared errors falls below a preselected minimum value. Linear regression techniques were then used to generate coefficients for the transformed variable (raised to nonlinear power coefficient). Statistically insignificant variables (t-statistic less than 2.0) were eliminated from the model. The nonlinear regression analysis to generate power coefficients and linear regression analysis to generate variable coefficients were repeated until all remaining variables were statistically significant in the prediction of joint faulting. The two joint faulting prediction models are presented below:

Doweled Joints

$$FAULT = (EROSION * 2)^{0.25} * [0.0032233 * \left(\frac{PRECIP}{10}\right)^{1.84121} + 0.0048573 * JS^{0.38274}] \quad \textbf{(35)}$$

where: $FAULT$ = Faulting at doweled transverse pavement joints, in.
$EROSION$ = Calculated accumulated erosion (Eqs. 3 & 4, Ref. 26), percent.
$PRECIP$ = Annual precipitation, in.
JS = Average joint spacing, ft.

statistics: $R^2_{adj} = 0.703$.
SEE (standard error of estimate) = 0.047 in.
n (no. of data points) = 281.

(Note: 1 in = 25.4 mm, 1 ft = 305 mm)

Aggregate-Interlock Joints

$$FAULT = EROSION^{0.25} * [9.75873 * 10^{-4} * (PRECIP)^{0.91907} + 0.0060291 * JS^{0.54428} - 0.016799 * DRAIN] \quad \textbf{(36)}$$

where: $FAULT$ = faulting at aggregate-interlock transverse pavement joints, in.
$EROSION$ = calculated accumulated erosion (Eqs. 3 & 4, Ref. 26), percent.
$PRECIP$ = annual precipitation, in.
JS = average joint spacing, ft.
$DRAIN$ = drainage dummy variable, 0 for none, 1 for edge drains.

statistics: $R^2_{adj} = 0.743$.
SEE (standard error of estimate) = 0.055 in.
n (no. of data points) = 582.

(Note: 1 in = 25.4 mm, 1 ft = 305 mm)

Detailed information related to the development of the above two models can be found in references 26 and 27.

Revision of the 1992 PCA Faulting Models

In addition to the variables used in the development of the 1992 PCA faulting models, other parameters, such as type of coarse aggregate, may be important in development of faulting in jointed concrete pavements. To account for these variables, attempts were made as part of this study to acquire additional information related to types of coarse aggregate used in the concrete for all the pavement sections used in developing the two equations. Both the coarse aggregate component and geology composition were identified. Types of aggregate component included gravel, crushed stone, slag, manufactured lightweight aggregate, and combinations of the above. For the pavement sections considered, the coarse aggregate was either gravel or crushed stone. This information was used in the revision of the faulting models. Coarse aggregate of different geologic composition will have different coefficients of thermal expansion. This information was used in calculating the joint opening for JPCP pavement sections that was used in the revision of the faulting prediction models.

With the additional variables included, the BMDP statistical analysis computer program was again used for the revision of the models. The procedure was similar to that used in the development of the original models (equations 35 and 36). Essentially, a non-linear regression technique was first performed on the data to determine the power terms of the equations. A linear regression technique was then used to determine the coefficients for the transformed variables.

Faulting at Aggregate-Interlock Joints

For aggregate-interlock joints, it was observed that coarse aggregate shape (round or crushed) had a significant effect on joint faulting. The use of crushed stone seemed to slow the progress of joint faulting compared with pavements with gravel aggregate. Even with the inclusion of different coefficient of thermal expansion values in computing the joint opening, there was no significant effect on the compacted faulting of aggregate-interlock joints. The revised faulting prediction equation for aggregate-interlock joints is as follows:

$$FAULT = EROSION^{0.25} * [-0.113924 * PRECIP^{-0.167423} + 0.0332380 * JS^{0.461035} - 0.0186867 * DRAIN - 0.0268094 * CAC] \quad (41)$$

where: $FAULT$ = Faulting at aggregate interlock transverse joints, in.
$EROSION$ = Calculated accumulated erosion (equations 5 & 6), percent.
$PRECIP$ = Annual precipitation, in.
JS = Average joint spacing, ft.
$DRAIN$ = Drainage dummy variable, 0 for none, 1 for edge drains.
CAC = Coarse aggregate component, 0 for gravel, 1 for crushed stone.

statistics: $R^2_{adj} = 0.766$.

SEE (standard error of estimate) = 0.048 in.
n (no. of data points) = 683.

(Note: 1 in = 25.4 mm, 1 ft = 305 mm)

Compared with the original 1992 PCA faulting prediction equation for aggregate-interlock joints, the revised equation shows some improvement in terms of both the adjusted coefficient of determination (R^2_{adj}) and the standard error of estimate (*SEE*). The revised prediction equation should therefore provide better estimation of joint faulting. As presented in figure 13, an approximately normal distribution centered around zero is observed for the prediction error.

For aggregate-interlock joints, a sensitivity analysis indicates that faulting increases with an increase in the value of the variable in question. Results of the sensitivity analysis for non-doweled joints are shown in table 8.

Table 8. Sensitivity of faulting to variable change for non-doweled joints.

Independent Variable	Effect on Faulting	Sensitivity
Increase in erosion	increase	varies with erosion
Increase in precipitation	increase	medium
Increase in joint spacing	increase	high
Use of crushed coarse aggregate	increase	medium
Use of edge drains	decrease	medium

Plots of faulting versus accumulated erosion for aggregate-interlock joints are shown in figures 14 through 17 for pavements using different coarse aggregate (crushed stone or gravel) and for pavements in wet regions (annual precipitation of 1016 mm) and in dry regions (annual precipitation of 508 mm).

The annual precipitation has a significant effect on joint faulting. For example, at 100 percent erosion for a 4.6-m-long slab in a region with an annual precipitation of 1016 mm the predicted joint faulting for a pavement using gravel coarse aggregate, as shown in figure 16, is 4.4 mm. For the same conditions but with a lower precipitation of 508 mm, the aggregate interlock model shown in figure 14 predicts faulting of 3.8 mm when no edge drains are present. A 50 percent reduction in precipitation results in a 14 percent reduction in faulting.

Joint spacing also has a significant effect on predicted aggregate-interlock joint faulting. For example, at 100 percent erosion for a 12.2-m-long slab in a region with an annual precipitation of 508 mm the predicted faulting for a pavement with gravel coarse aggregate, as shown in figure 14, is 9.1 mm when edge drains are not used. For the same conditions but with a smaller joint spacing of 4.6 m the aggregate-interlock joint model, as shown in figure 14, predicts faulting of 3.8 mm. A 63 percent reduction in joint spacing results in a 58 percent reduction in faulting.

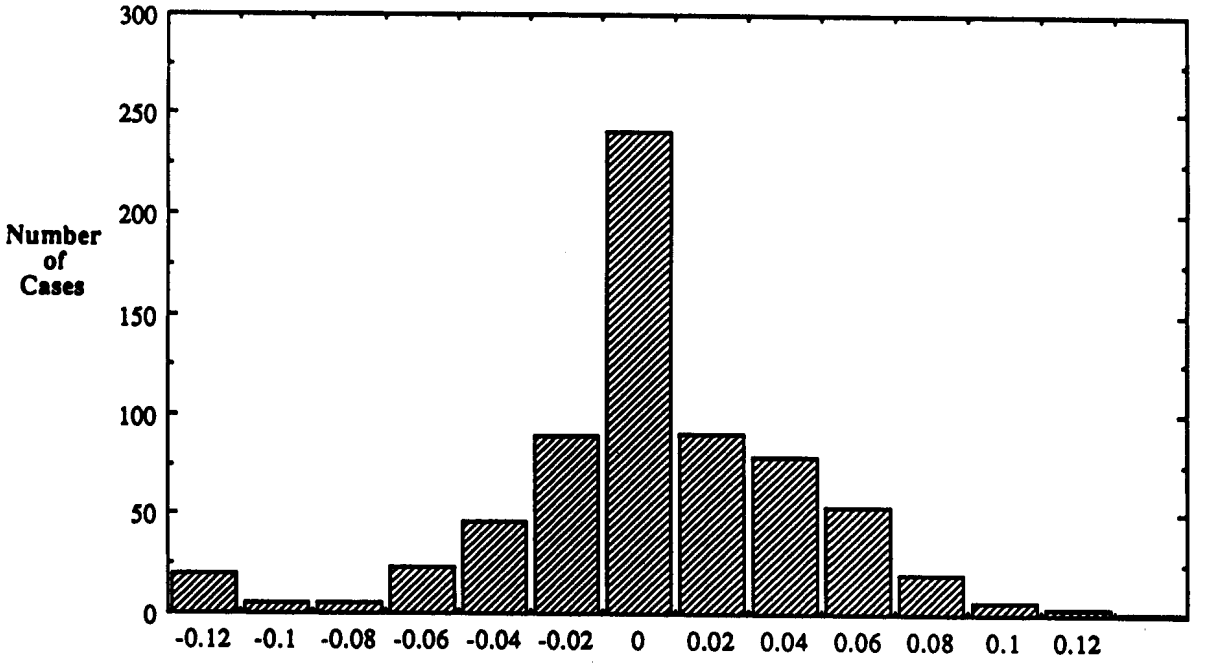

(1 in = 25.4 mm)

Figure 13. Faulting prediction error distribution for aggregate-interlock joints.

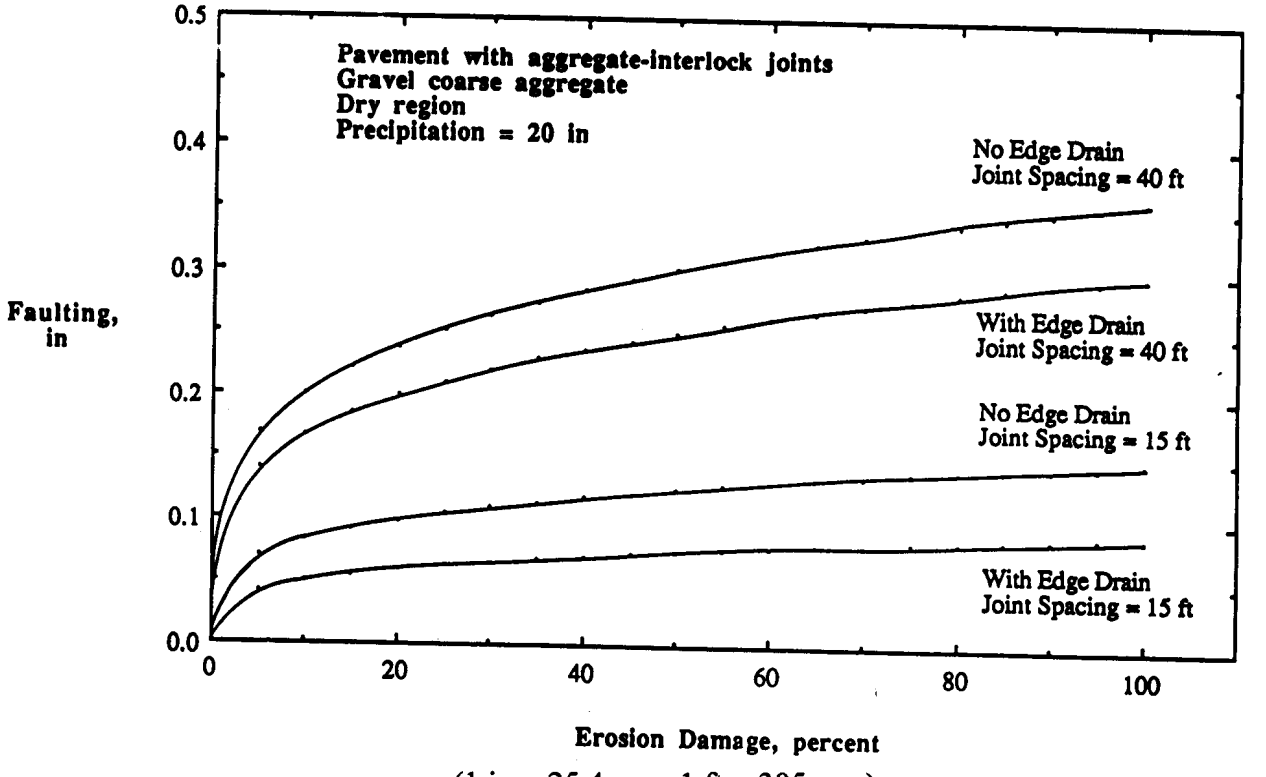

(1 in = 25.4 mm, 1 ft = 305 mm)

Figure 14. Faulting versus accumulated erosion for aggregate-interlock joints with gravel coarse aggregate in dry region.

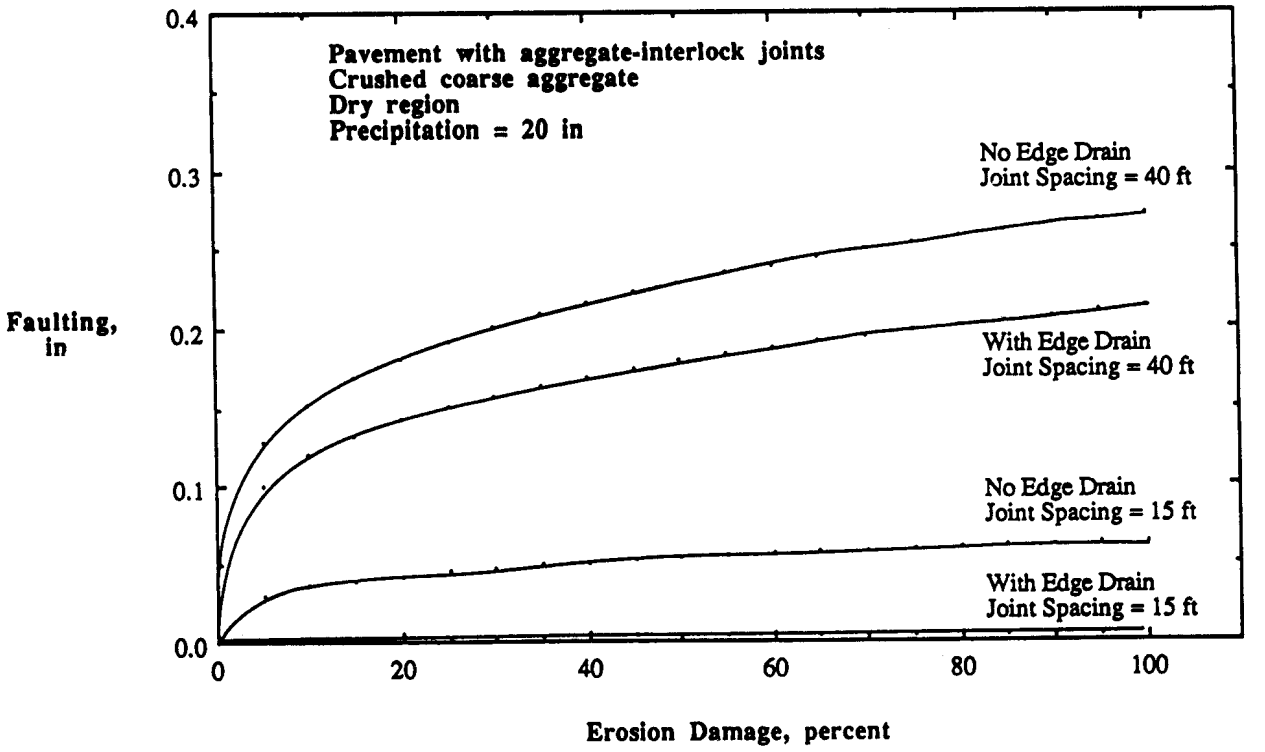

(1 in = 25.4 mm, 1 ft = 305 mm)

Figure 15. Faulting versus accumulated erosion for aggregate-interlock joints with crushed coarse aggregate in dry region.

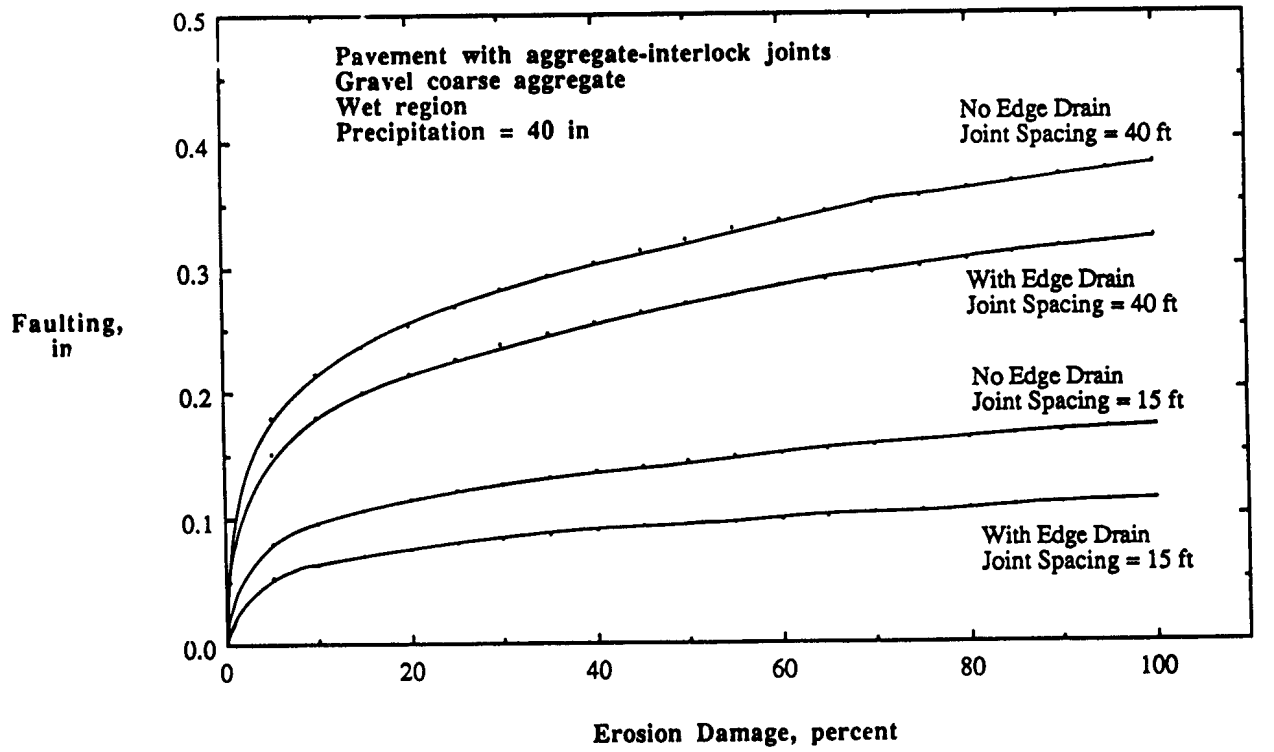

(1 in = 25.4 mm, 1 ft = 305 mm)

Figure 16. Faulting versus accumulated erosion for aggregate-interlock joints with gravel coarse aggregate in wet region.

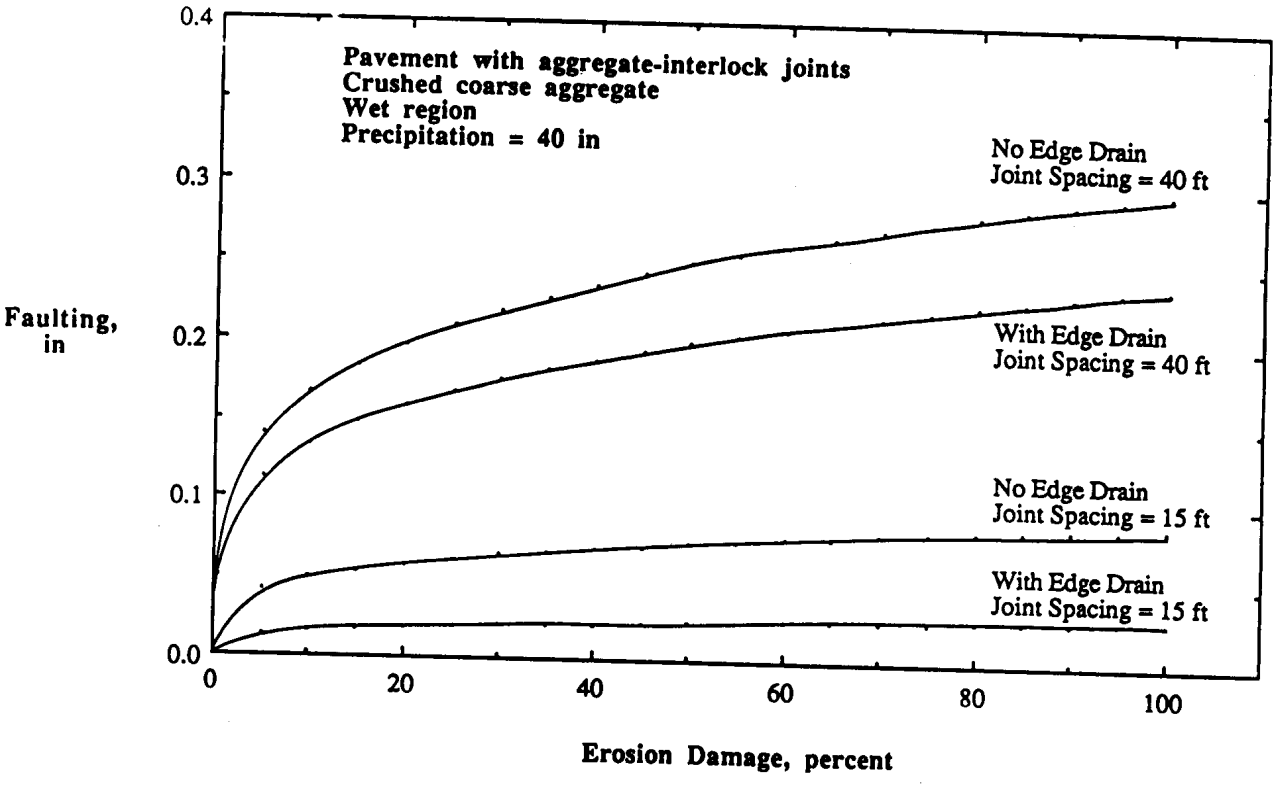

(1 in = 25.4 mm, 1 ft = 305 mm)

Figure 17. Faulting versus accumulated erosion for aggregate-interlock joints with crushed coarse aggregate in wet region.

Also shown in these figures, the use of longitudinal edge drains and the use of crushed stone coarse aggregate were statistically significant in reducing aggregate interlock joint faulting. However, the effectiveness of these two parameters in reducing aggregate-interlock faulting is dependent on the percent erosion level. They become more effective as percent erosion increases.

Faulting at Doweled Joints

For pavements with doweled joints, statistical analysis showed that the coarse aggregate type (crushed stone or gravel) had significant effects on the predicted joint faulting. However, when compared with the 1992 PCA faulting prediction equation, the new prediction equation, with the inclusion of coarse aggregate type as a predictor, had lower R^2_{adj} (0.648) and higher *SEE* (0.072). It was therefore determined that the coarse aggregate type need not be included as a predictor in estimating faulting for doweled joints. Instead, the 1992 PCA faulting prediction equation (equation 35) was selected for use in this study. The equation is given below:

$$FAULT = (EROSION * 2)^{0.25} * 0.0032233 * \left(\frac{PRECIP}{10}\right)^{1.84121} + 0.0048573 * JS^{0.38274} \quad (42)$$

where: *FAULT* = Faulting at doweled transverse pavement joints, in.
EROSION = Calculated accumulated erosion (equations 5 and 6), percent.
PRECIP = Annual precipitation, in.
JS = Average joint spacing, ft.

statistics: $R^2_{adj} = 0.703$.
SEE (standard error of estimate) = 0.047 in.
n (no. of data points) = 281.

(Note: 1 in = 25.4 mm, 1 ft = 305 mm)

The predicted faulting error distribution is shown in figure 18. Again, the prediction errors are symmetrically distributed around zero.

Similar to the aggregate-interlock joints, a sensitivity analysis indicates that faulting increases with an increase in the value of the variable in question. Results of the sensitivity analysis for doweled joints are shown in table 9.

Table 9. Sensitivity of faulting to variable change for doweled joints.

Independent Variable	Effect on Faulting	Sensitivity
Increase in erosion	increase	varies with erosion
Increase in precipitation	increase	high
Increase in joint spacing	increase	medium

Plots of faulting versus accumulated erosion are shown in figures 19 and 20 for wet regions (annual precipitation of 1016 mm) and dry regions (annual precipitation of 508 mm), respectively. Figures 14 through 17, 19 and 20 should not directly be used for comparing the effectiveness of dowel bars in reducing faulting since they are plotted as a function of erosion. Erosion is computed using erosion factors that include the benefits (higher amount of allowable loads) of dowel bars.

Again, the annual precipitation has a significant effect on joint faulting for doweled joints. For example, at 100 percent erosion for a 4.6-m-long slab in a region with an annual precipitation of 1016 mm the predicted faulting as shown in figure 19, is 5.3 mm. For the same conditions but with a lower precipitation of 508 mm the doweled model shown in figure 20 predicts faulting of 2.4 mm. A 50 percent reduction in precipitation results in a 50 percent reduction in faulting.

Joint spacing also has a significant effect on predicted faulting. For example, at 100 percent erosion for a 12.2-m-long slab in a region with an annual precipitation of 508 mm the predicted faulting for doweled joints, as shown in figure 20, is 3.0 mm. For the same conditions but with a smaller joint spacing of 4.6 m the doweled joint model shown in figure 20 predicts faulting of 2.4 mm. A 63 percent reduction in joint spacing results in a 19 percent reduction in faulting.

Evaluation of the Revised 1992 PCA Faulting Models Using SHRP LTPP Data (GPS-3 and GPS-4)

Data obtained from the LTPP data base for GPS-3 (JPCP) and GPS-4 (JRCP) test sections were used in evaluating the revised faulting models. Types of information required from the LTPP data base included the following:

- Pavement structural design parameters
  - PCC thickness
  - PCC modulus of elasticity
  - Modulus of subgrade reaction
  - Coarse aggregate types
  - Type and thickness of base or subbase layers
  - Type of pavement shoulder
  - Joint type, doweled or aggregate-interlock
  - Average joint spacing
- Drainage type
- Traffic information
  - Axle load distribution
- Climatic data
  - Annual precipitation
  - Freezing index

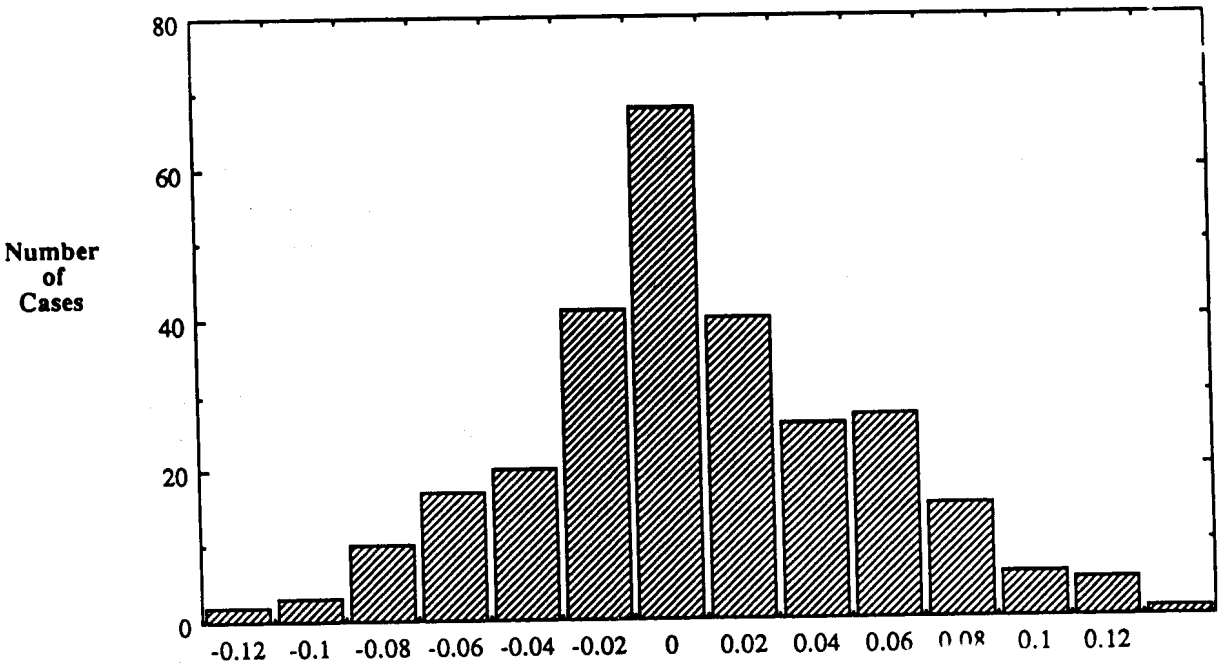

Figure 18. Faulting prediction error distribution for doweled joints.

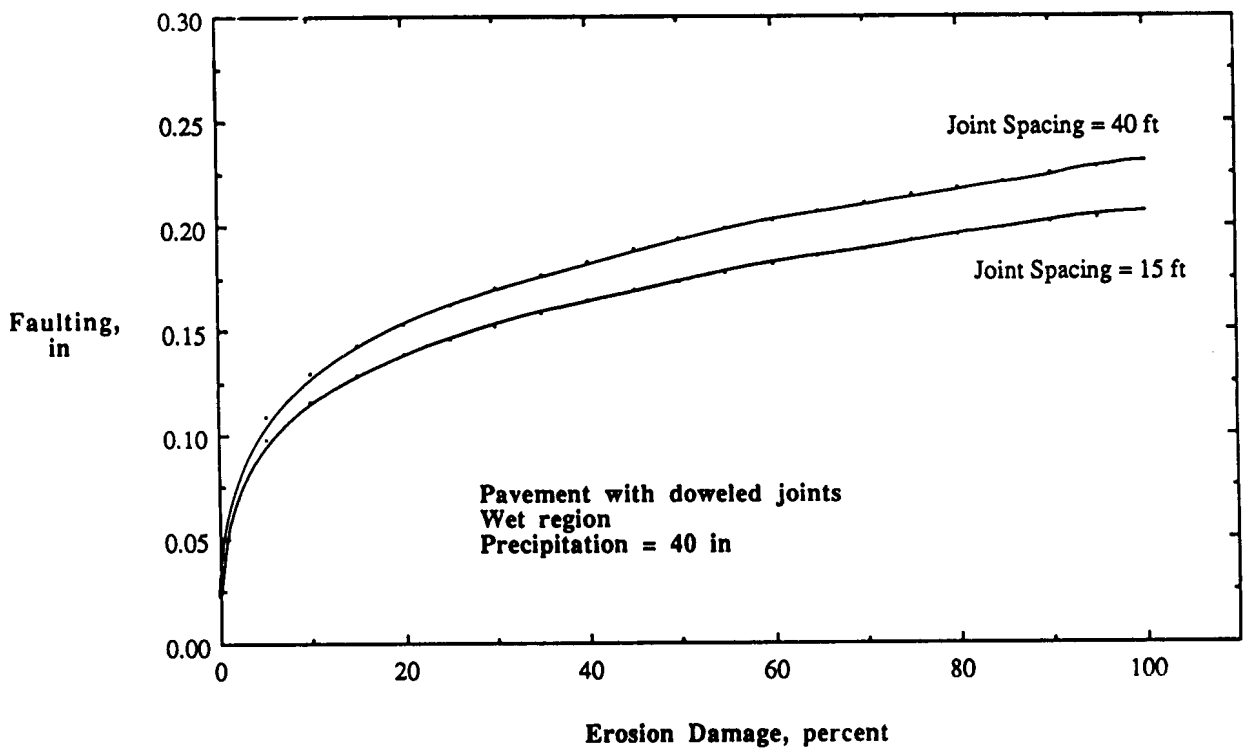

(1 in = 25.4 mm, 1 ft = 305 mm)

Figure 19. Faulting versus accumulated erosion for doweled joints in wet region.

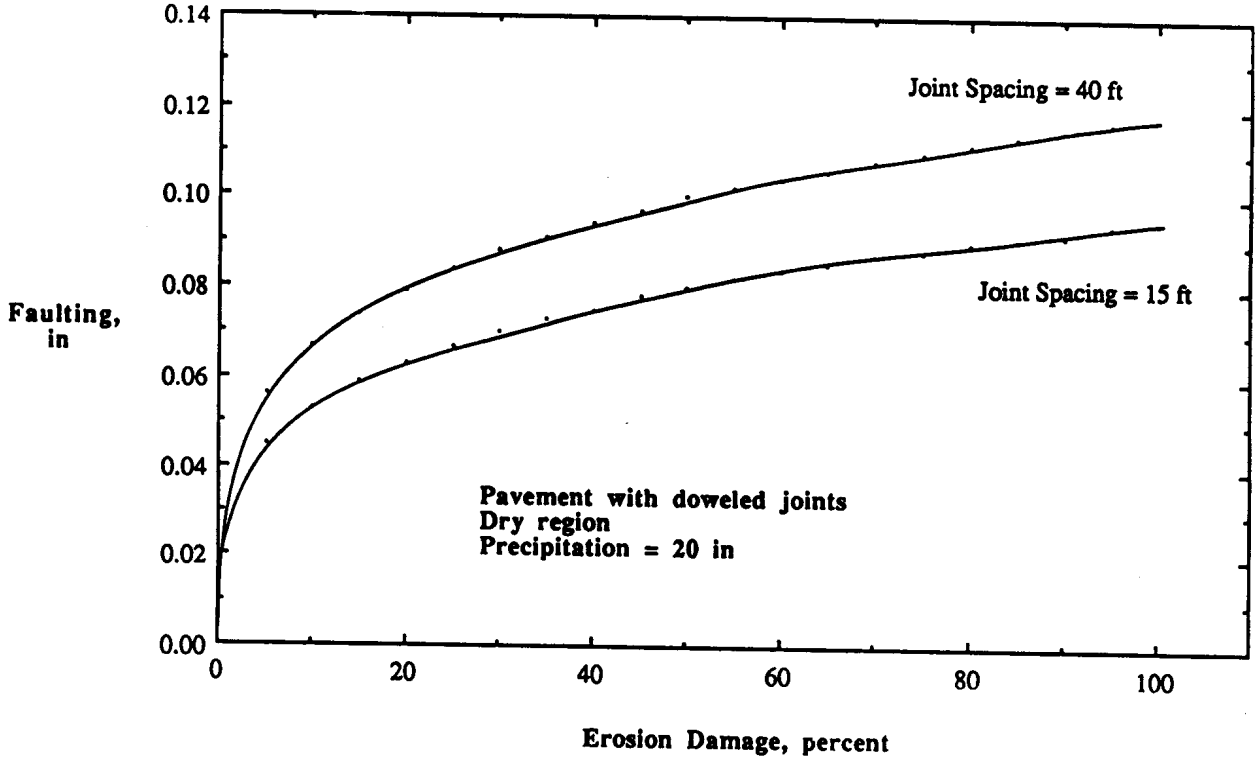

(1 in = 25.4 mm, 1 ft = 305 mm)

Figure 20. Faulting versus accumulated erosion for doweled joints in dry region.

- Date pavement opened to traffic and date of faulting measurement
- Faulting measurement data

Most of the data were extracted from the data base (as discussed in chapter 2) and directly used in the analysis. However, some manipulation was required for some of the data before they could be used in the evaluation process.

PCC Modulus of Elasticity

Attempts were first made to use the measured concrete modulus of elasticity data in the evaluation. However, too many missing data made this approach impossible. As the second step, PCC moduli of elasticity backcalculated from falling weight deflectometer (FWD) test data were considered. However, a closer examination of the backcalculated concrete modulus values revealed that most of the values were much too high, with some reaching 90,000 MPa . Since the computed erosion factor caused by traffic loads on pavement systems will be affected by the concrete modulus of elasticity, the use of unrealistically high values was considered inadequate.

For the purpose of this analysis, the best possible material testing data available at the time of analysis appeared to be the 28-day compressive strength of concrete specimens. For most of the test sections evaluated in this study, the 28-day compressive strength data were used to estimate concrete modulus of elasticity. For a few cases, the 28-day compressive strength data were not available and the concrete modulus of rupture (flexural strength) data were used to estimate the modulus of elasticity values for that section.

Modulus of Subgrade Reaction

The modulus of subgrade reaction values backcalculated from FWD deflection tests were available for all the pavement sections considered in this analysis. For pavements with a stabilized or granular base or subbase layer, their backcalculated k-values were adjusted to account for the increased support provided by the presence of base and/or subbase layers using the PCA thickness design guideline procedures.[29]

Traffic Data

To compute the accumulated erosion of a pavement system, the axle load distribution over its service life for all the weight categories is required. Unfortunately, very limited traffic data were available. The lack of axle load distribution data reduced the number of test sections that could be evaluated. A total of 57 pavement sections were included in this study, consisting of 20 pavements with aggregate-interlock joints and 37 with doweled joints. Furthermore, the data available were mostly for a single year only. To estimate the total amount of traffic traveled on a pavement during its entire service life, an annual traffic increase rate of 2 percent was assumed in the analysis (as discussed in chapter 2). This assumption somewhat overestimates the joint faulting. The effect of annual traffic growth rate on the predicted joint faulting is presented in a latter section.

Predicted Faulting versus Measured Faulting for Aggregate-Interlock Joints

With all the information obtained and derived from the LTPP data base, the predicted faulting for aggregate-interlock joints was computed using the revised 1992 joint faulting equation. As mentioned earlier, complete information was obtained for 20 pavement sections. The differences between the predicted and observed faulting (prediction errors) ranged from -1.5 mm to 1.32 mm, with a mean value of -0.76 mm and a standard deviation of 0.79 mm. As presented in figure 21, the prediction errors are distributed approximately symmetrically around zero, indicating reasonable predicting power of the faulting model.

A paired-t test also was performed to further evaluate the adequacy of the prediction equation. It was concluded that, at the 95 percent confidence level, the null hypothesis of no difference between the predicted and observed faulting could not be rejected. In fact, the null hypothesis could not be rejected even at the 70 percent confidence level. This conclusion suggested that the developed faulting prediction model is reasonable for predicting faulting for aggregate-interlock joints. The comparison of the predicted and the observed faulting for aggregate-interlock joints is shown in figure 22. In the figure, the solid line represents the line of equality and the two dashed lines are one standard deviation away from the line of equality. It is observed that most of the data points fall within ±1 standard deviation from the line of equality.

Predicted Faulting versus Measured Faulting for Doweled Joints

Joint faulting was computed using the 1992 joint faulting equation and data obtained from the LTPP data base for doweled joints. A total of 37 pavement sections having the needed data were evaluated. The differences between the predicted and observed faulting (prediction errors) ranged from -1.7 mm to 3.0 mm, with a mean value of 0.56 mm and a standard deviation of 1.24 mm. Plotted in figure 23, the prediction error distribution for doweled joints shows skewness toward the positive side, indicating an overestimate of the predicted faulting. A paired-t test further revealed that the null hypothesis of no difference between the predicted and observed faulting was rejected at the 95 percent confidence level. It can therefore be inferred that there is a difference between the predicted and observed faulting.

The predicted faulting is plotted against the observed faulting in figure 24. It is observed that most of the measured faulting values are in the range between 0.00 and 1.27 mm. The use of doweled joints seemed to significantly reduce joint faulting. It is also clear that, at this lower range, the prediction equation tends to overestimate joint faulting for doweled joints. For measured faulting greater than 1.27 mm, the equation seems to provide better faulting estimates for doweled joints.

Discussion of Results

As presented in the previous sections, the aggregate-interlock model provided reasonably good estimates for joint faulting for the 20 LTPP sections evaluated. Statistically, no difference could be claimed between the predicted and observed faulting for aggregate-interlock joints. However, an overestimate of the faulting was evident for doweled joints, as indicated by the positive skewness of the faulting prediction error distribution shown in figure 23.

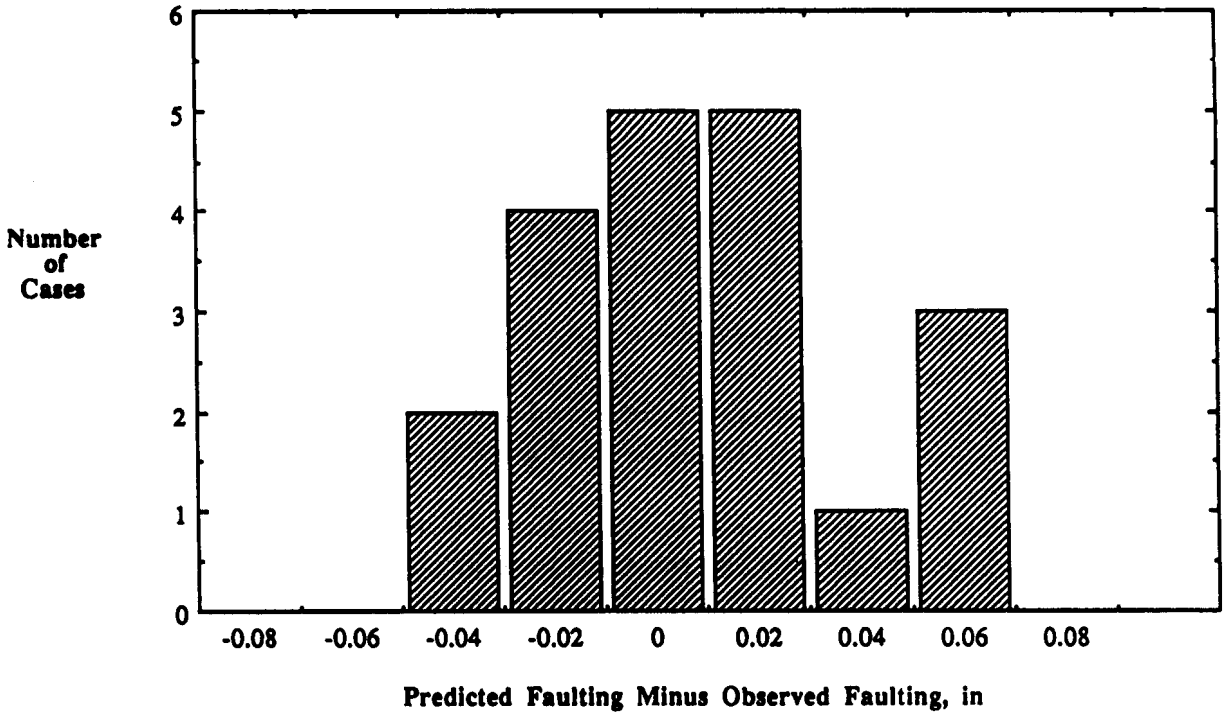

(1 in = 25.4 mm)

Figure 21. Faulting prediction error distribution for aggregate-interlock joints.

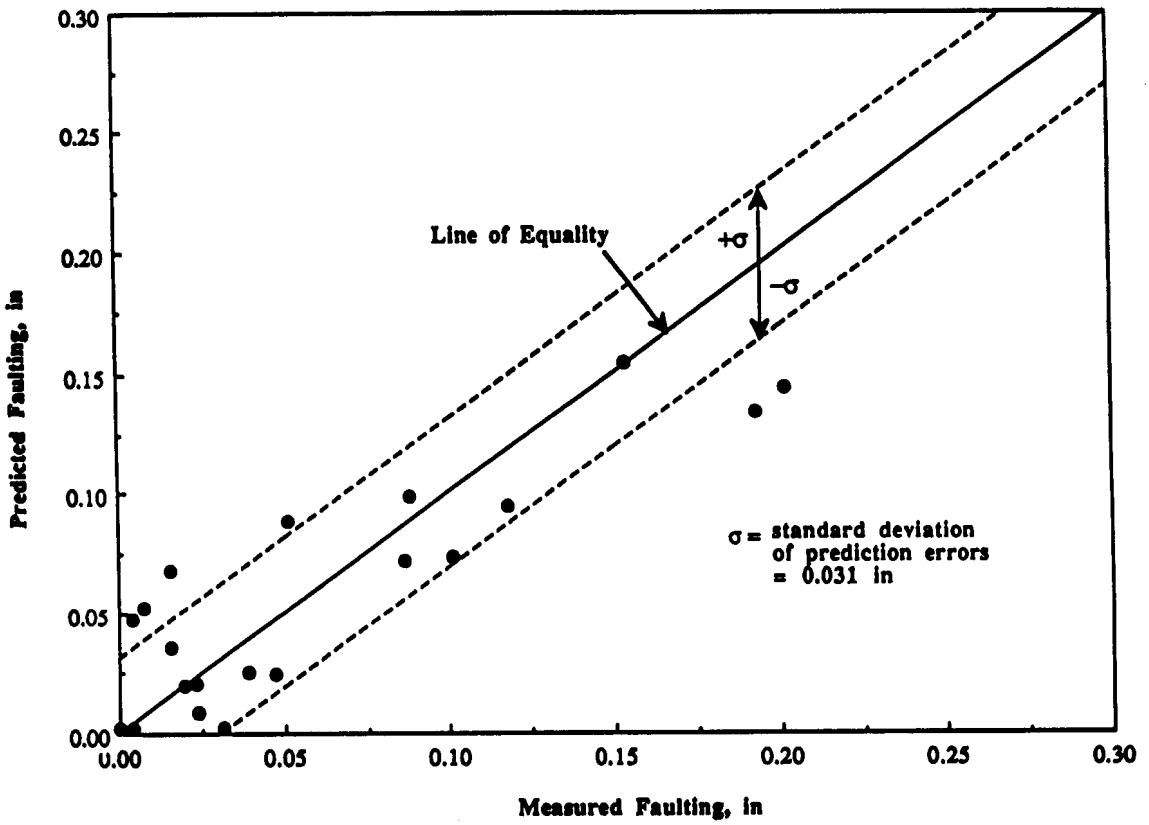

(1 in = 25.4 mm)

Figure 22. Predicted faulting versus measured faulting for aggregate-interlock joints.

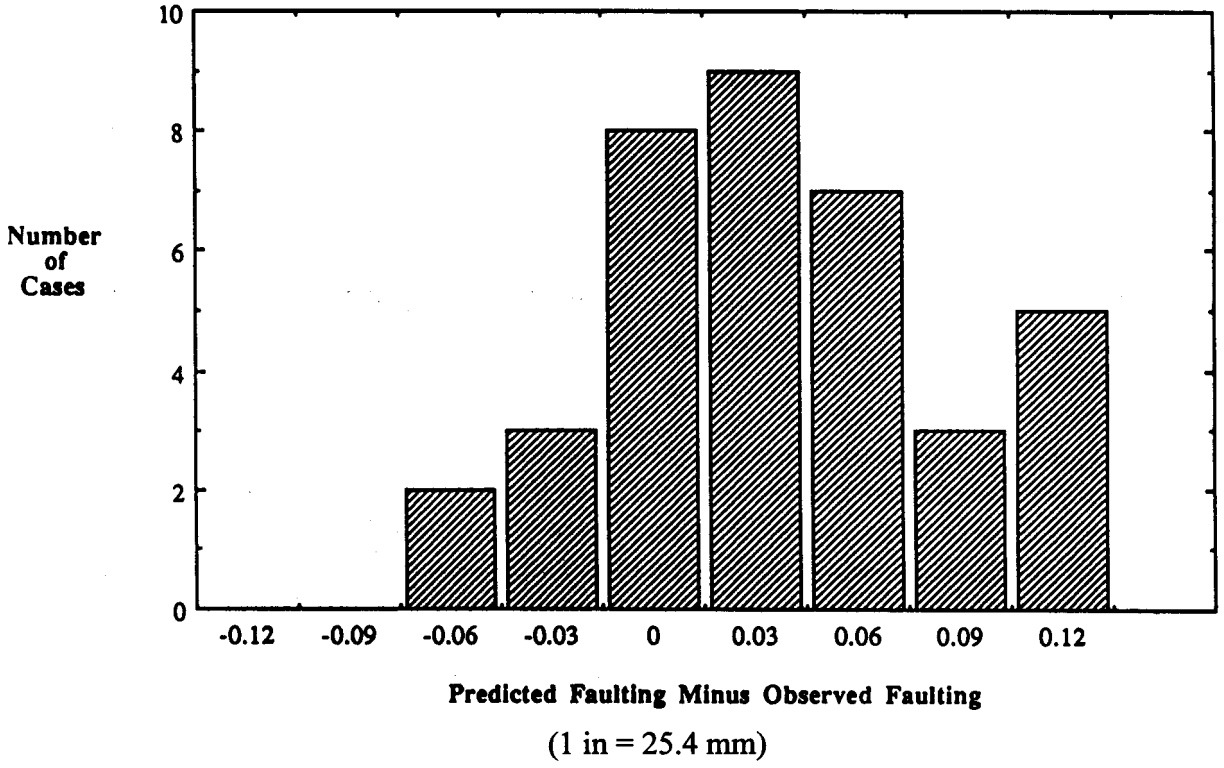

(1 in = 25.4 mm)

Figure 23. Faulting prediction error distribution for doweled joints.

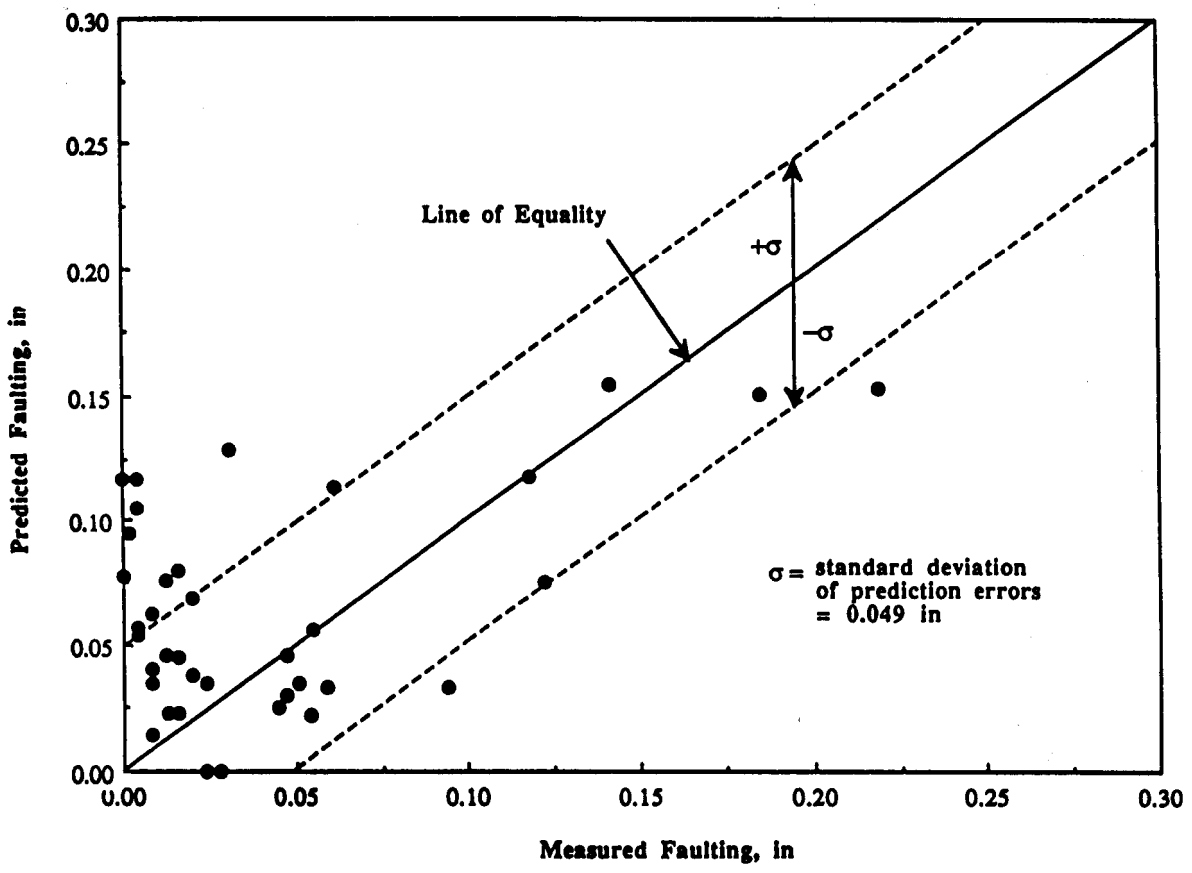

(1 in = 25.4 mm)

Figure 24. Predicted faulting versus measured faulting for doweled joints.

The PCA faulting prediction equation utilizes the concept of erosion damage of the pavements caused by traffic loads. Erosion damage is determined based on traffic load-induced corner deflections in the pavements. Among other parameters, concrete modulus of elasticity is important in determining the corner deflections. However, site specific data were not available at the time of analysis. In this study, concrete modulus of elasticity was estimated from its 28-day compressive strength. It is believed that use of actual measured concrete modulus of elasticity data will increase the prediction accuracy.

Similar to other mechanistic-based procedures, the joint faulting prediction equations require the use of traffic axle load distribution in the analysis. Converted traffic indices, such as 80-kN ESAL currently used in the AASHTO design procedure, cannot be used. At the time of analysis, the LTPP data base contained traffic axle load distribution data for a very limited number of pavement sections. Furthermore, for these limited number of test sections, axle load distribution data were only available for a particular year, and the cumulative amount of traffic volume on the pavements had to be estimated using a 2 percent annual traffic growth rate, as discussed in chapter 2. This assumption was believed to be conservative and might have contributed to the overestimate of the doweled joint faulting. Reliable traffic data (in terms of axle loadings) are essential for any pavement evaluation using the LTPP data base.

Sensitivity analyses of annual traffic growth rate on computed faulting were performed for both doweled and aggregate-interlock joints, and are presented in figure 25. It can be observed that traffic growth rate only slightly affects the predicted faulting for both types of joints. As the annual traffic growth rate increases from 2 to 15 percent, the computed faulting decreases from 1.32 mm to 1.14 mm and from 1.60 mm to 1.50 mm for the aggregate-interlock joint and the doweled joint, respectively. It should be noted that because traffic is backcasted from a current year, higher growth rates result in lower cumulative traffic loadings. The prediction errors may be reduced slightly if annual growth rate of traffic can be estimated reliably.

The lack of required material testing and traffic data reduced the number of LTPP test sections that could be evaluated. However, the quality of the faulting data may be a more serious deficiency of the data base. For instance, faulting observed at two consecutive years at many sections had a difference in excess of 2.54 mm. In some cases, faulting measured at the wheel path was very different from that measured at the corner. These inconsistencies make the use of the LTPP data difficult. The following are a few examples of inconsistencies of the faulting data:

- Pavement section 1-3028
  Faulting at wheel path: 0.000 mm
  Faulting at corner: 3.28 mm

- Pavement section 12-4138
  Faulting at wheel path: 0.000 mm
  Faulting at corner: 5.13 mm

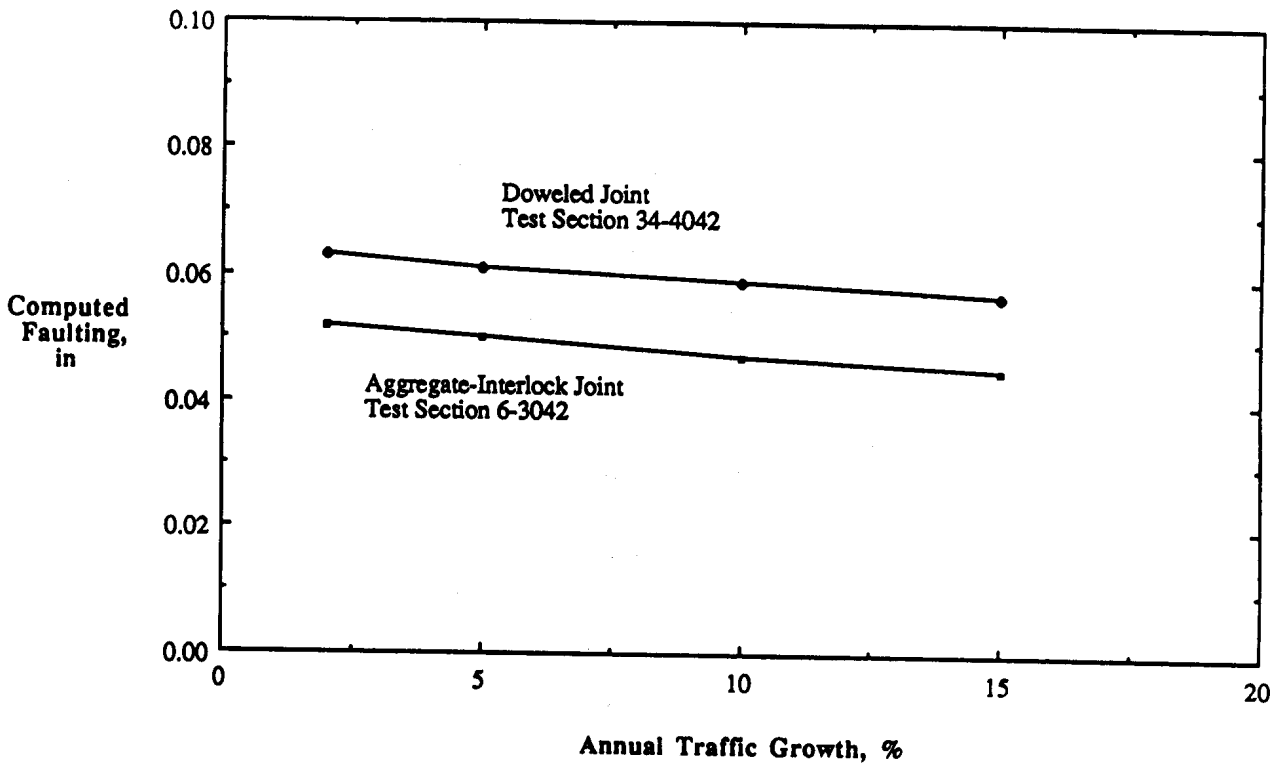

(1 in = 25.4 mm)

Figure 25. Sensitivity analysis of annual traffic growth rate on computed faulting.

- Pavement section 1-4084
  Faulting measured in 1991 (21 years): 4.29 mm
  Faulting measured in 1993 (23 years): 8.79 mm

- Pavement section 34-4042
  Faulting measured in 1991 (24 years): 4.70 mm
  Faulting measured in 1992 (25 years): 5.56 mm
  Faulting measured in 1993 (26 years): 3.58 mm

In general, the LTPP data base provides valuable information that can be used to develop, calibrate, and/or validate mechanistic-based pavement analysis and design procedures. However, the issues of lack of material testing and traffic data, and the quality of the performance data need to be addressed.

Summary

The two faulting prediction models, one for aggregate-interlock joints and the other for doweled joints, developed in 1992 were revised in an attempt to include coarse aggregated type as a predictor. Reasonable coefficients of determination (greater than 0.70) were obtained. For doweled joints, important factors that will influence faulting include erosion, precipitation, and joint spacing. For aggregate-interlock joints, erosion, precipitation, joint spacing, the use of edge drains, and coarse aggregate types were found to be significant in affecting joint faulting.

Sensitivity analyses of the two joint faulting prediction equations have revealed that faulting will increase with increased erosion, precipitation, or joint spacing for both doweled and aggregate-interlock joints. The use of edge drains and crushed stone coarse aggregate will reduce faulting.

The two faulting prediction equations were evaluated using data obtained from GPS-3 and GPS-4 test sections. A total of 57 pavement sections, consisting of 20 aggregate-interlock joints and 37 doweled joints, were evaluated. The prediction equation for aggregate-interlock joints was found to provide reasonable estimates of joint faulting compared with the observed values. However, an overestimate, especially in the lower range of measured faulting of less than 1.27 mm, was observed for doweled joints.

CHAPTER 5 - SUMMARY AND RECOMMENDATIONS

General Observations

The primary objective of the study reported here was to evaluate the reliability of some widely used M-E models for predicting the performance of in-service PCC pavements. Two distress types were considered in this study: fatigue cracking for jointed plain concrete pavements and joint faulting for jointed plain and reinforced concrete pavements. Another objective was to develop and calibrate new performance prediction models, as deemed necessary.

Prediction of Fatigue Cracking and Joint Faulting Using Mechanistic Procedures

The following are some important observations based on the results of the study:

- Both the NCHRP 1-26 approach for prediction of fatigue cracking (based on cracking initiating at slab bottom) and the PCA type approach for prediction of joint faulting appear reasonable within the context of the validation attempted using LTPP test data. However, as more data become available, it may also be possible to consider other hypotheses for development of fatigue cracking in jointed concrete pavements.

- The PCA joint faulting procedure incorporates mechanistic elements (especially the "damage" caused by the different axle loads), but is also dependent on certain site-specific features. In an ideal mechanistic approach, all site-specific features should be incorporated within the mechanistic parameters that represent the structural characteristics of the pavement, specifically within seasonally adjusted modulus of elasticity values for the various paving materials.

- The incorporation of curling and warping effects in both the fatigue cracking analysis and the joint faulting analysis need major advancement. This is especially true with regard to the assumption of linear temperature gradient in the concrete slab and the complete omission of moisture warping stresses. Similarly, better understanding of how to estimate loss of support and joint load transfer effectiveness and how to incorporate these estimates into the structural analysis is needed. The estimate of the fatigue cracking damage is very sensitive to the computation of the total flexural (bending) stresses in the slab. Also, consideration of the loss of support and load transfer effectiveness can significantly affect the estimate of the faulting damage.

- The development of joint faulting is very similar to that of rutting in asphalt pavements. The rate of faulting is high in the early years and decreases with time. No practical approaches have been developed to allow consideration of this non-linear relationship between faulting and the number of load applications.

LTPP Data Issues

Issues relating to the specific data types are discussed in the following paragraphs. The purpose of this discussion is to provide feedback to the LTPP data collection efforts, help identify areas of improvement needed in the data collection effort, and identify future research needs to fill data and knowledge gaps within the context of the M-E analysis/design procedures.

Materials Data

The key materials data needed for both the fatigue cracking and joint faulting analysis include concrete modulus of elasticity values, the coefficient of subgrade reaction, the concrete coefficient of thermal expansion, and the concrete flexural strength values. As indicated previously, at the time of the study, the site-specific coefficient of thermal expansion values were not available and a single value was used for all test sections. Also, the concrete modulus of elasticity and flexural strength values were extrapolated. No seasonal adjustments were made to these values nor were long-term aging effects considered. The backcalculated layer moduli values for concrete were not considered appropriate because many of these values were higher than normally expected. Finally, material variability effects were not considered. Future improvements are needed to establish these values to be used for M-E data analysis.

Traffic Data

In this analysis, traffic was characterized as annual counts of an array of specific axle loading groups. The analysis is thus complicated, since there are up to 140 axle loading groups in the LTPP data base. Although it is conceivable that individual loading groups may have different growth rates, a simplifying assumption was made that the annual traffic growth rate is 2 percent for all load groups. Also, another assumption that needs further study is the seasonal variation in traffic load applications to ensure that seasonal traffic is matched to seasonal variation in the structural properties of the various pavement layers. Finally, traffic wander (lateral distribution) needs to be established for each site to ensure that appropriate traffic data are used for both the fatigue analysis and the faulting analysis.

Distress Data

Concerns remain about the quality of the distress data. These concerns include the following:

1. Removal of random cracking from the fatigue cracking data.

2. Cleaning up the joint faulting data, including discrepancies between faulting magnitudes at corner locations versus wheelpath locations and a few cases of negative faulting values.

Summary

In an ideal M-E procedure, damage (in relation to a specific distress) should be determined as follows:

$$Damage_{ijk\ell} = f\left(e_{ijk\ell}\right) \quad \text{and} \quad e_{ijk\ell} = f\left(E_{jk\ell}\right) \tag{42}$$

where: $e_{ijk\ell}$ = Critical structural response in the pavement that is considered to be a predictor of the distress under consideration for the ith axle group at the jth time period of the kth month of the ℓth year.

$E_{jk\ell}$ = Modulus of elasticity of each layer of the pavement system at the jth time period of the kth month of the ℓth year.

Thus, a major consideration in developing and using M-E procedures is the appropriate characterization of $E_{jk\ell}$ for each pavement layer. Our capability for realistically modeling pavement behavior has seen much progress in the last few decades. However, the capability to realistically consider material characterization (e.g., $E_{jk\ell}$) for the pavement layers remains less than desired because of the lack of knowledge of how to realistically account for seasonality effects, spatial variability, and effects of deterioration due to traffic loading and environment.

In this study, distress-specific damage was estimated for a segment of LTPP test sections. However, as discussed in the report, the damage estimation was seriously handicapped by two primary factors: lack of adequate (in terms of reliability and completeness) traffic data and the many approximations that had to be made to develop an appropriate characterization of the pavement layer properties (in terms of $E_{jk\ell}$). Future endeavors in the LTPP and other pavement research programs will attempt to improve these serious inadequacies.

The LTPP data base is one of the most important advances made in improving pavement technologies. This study has shown that, even given the many limitations, the LTPP data can be used successfully to develop better insight into pavement behavior and to ultimately improve pavement performance.

REFERENCES

1. Rowshan, S., and Harris, S., *Long-Term Pavement Performance Information Management System Data Users Guide*, FHWA-RD-93-094, Federal Highway Administration, Washington, DC, 1993.

2. Hammitt, G.M., II, *Concrete Strength Relationships*, U.S. Army Corps of Engineers Waterways Experiment Station, Vicksburg, MS, 1971.

3. Darter, M.I., and Barenberg, E.J., *Design of Zero-Maintenance Plain Jointed Concrete Pavement, Volume 1—Development of Design Procedures*, FHWA-RD-77-111, Washington, DC, 1977.

4. Mindess, S., and Young, J.F., *Concrete*, Prentice-Hall, Inc., Englewood Cliffs, NJ, 1981.

5. Hall, K.T., Darter M.I., Hoerner, T.E., and Khazanovich, L., *LTPP Data Analysis, Phase I: Validation of Guidelines for k Value Selection and Concrete Pavement Performance Prediction*, Interim Report, DTFH61-94-C-00218, Federal Highway Administration, Washington, DC, 1996.

6. Emery, D.K., *A Preliminary Report on the Transverse Lane Displacement for Design Trucks on Rural Freeways*, Paper presented to the ASCE Pavement Design Speciality Conference, Atlanta, GA, June, 1975.

7. Benekohal, R.F., Hall, K.T., and Miller, H.W., *Effects of Lane Widening on Lateral Distribution of Truck Wheels*, Transportation Research Record 1286, Transportation Research Board, Washington, DC, 1990.

8. Dempsey, B.J., Herlache, W.A., and Patel, A.J., *The Climatic-Materials-Structural Pavement Analysis Program User's Manual*, FHWA/RD-82/126, Federal Highway Administration, Washington, DC, 1986.

9. Salsilli, R.A., Barenberg, E.J., and Darter, M.I., *Calibrated Mechanistic Design Procedure to Prevent Transverse Cracking of Jointed Plain Concrete Pavements*, Proceedings of the 5th International Conference on Concrete Pavement Design and Rehabilitation, Purdue University, 1993.

10. Tabatabaie-Raissi, A.M., *Structural Analysis of Concrete Pavement Joint*, Ph.D. Thesis, University of Illinois, Urbana, 1977.

11. Ioannides, A.M., Thompson, M.R., and Barenberg, E.J., *Finite Element Analysis of Slab-on-Grade Using a Variety of Support Models*, Proceedings of the Third International Conference on Concrete Pavement Design and Rehabilitation, Purdue University, 1985.

12. Korovesis, G.T., *Analysis of Slabs-on-Grade Pavement Systems Subjected to Wheel and Temperature Loadings*, Ph.D. Thesis, University of Illinois, Urbana, Illinois, 1990.

13. Westergaard, H.M., "New Formulas for Stresses in Concrete Pavements of Airfields," *Transactions*, American Society of Civil Engineers, Volume 113, 1948.

14. Ioannides, A.M., Thompson, M.R., and Barenberg, E.J., *Westergaard Solutions Reconsidered*, Transportation Research Record 1043, Transportation Research Board, Washington, DC, 1985.

15. Bradbury, R.D., *Reinforced Concrete Pavements*, Wire Reinforcement Institute, 1938.

16. Westergaard, H.M., "Analysis of Stresses in Concrete Pavements Due to Variations of Temperature," *Proceedings*, Sixth Annual Meeting, Highway Research Board, Washington, DC, 1926.

17. Yu, H.T., Darter, M.I., Smith, K.D., Jiang, Y.J., and Khazanovich, L., *Performance of Jointed Concrete Pavements, Volume III: Improving Concrete Pavement Performance*, Final Report, DTFH61-91-C-0053, Federal Highway Administration, Washington, DC, August 1996.

18. *The AASHO Road Test*, Highway Research Board Special Report No. 61E, Transportation Research Board, Washington, DC, 1962.

19. Packard, R.G., and Tayabji, S.D., *Mechanistic Design of Concrete Pavements to Control Joint Faulting and Subbase Erosion*, Paper presented at the International Seminar on Drainage and Erodability at the Concrete Slab-Subbase-Shoulder Interfaces, Paris, France, March 1983.

20. *Computer Program for the Analysis and Design of Foundation Mats and Combined Footings*, SR100D, Portland Cement Association, Skokie, Illinois, 1971.

21. Darter, M.I., Becker, J.M., and Smith, R.E., *Portland Cement Concrete Pavement Evaluation System COPES*, Report prepared by the University of Illinois, Urbana-Champaign, for the National Cooperative Highway Research Program (NCHRP), Report 277, September 1985.

22. Smith, K.D., Mueller, A.L., Darter, M.I., and Peshkin, D.G., *Performance of Jointed Concrete Pavements*, Volumes I through VI, Report prepared by ERES Consultants, Inc., for the Federal Highway Administration (FHWA), FHWA/RD-89/136 through 89/141, Washington DC, July 1990.

23. Majidzadeh, K., and Ilves, G.J., *Correlation of Quality Control Criteria and Performance of PCC Pavements*, Report prepared by Resource International, Inc., for the Federal Highway Administration (FHWA), FHWA/RD-83/014, Washington DC, March 1984.

24. Heinrichs, K.W., Liu, M.I., Darter, M.I., Carpenter, S.H., and Ioannides, A.M., *Rigid Pavement Analysis and Design*, Report prepared by the University of Illinois, Urbana-

Champaign, for the Federal Highway Administration (FHWA), FHWA/RD-88-068, Washington DC, June 1989.

25. *Thickness Design for Concrete Highway and Street Pavements*, Portland Cement Association, Engineering Bulletin EB109.01P, Skokie, Illinois, 1984.

26. Wu, C.L., and Okamoto, P.A., *Refinement of the Portland Cement Association Thickness Design Procedure for Concrete Highway and Street Pavements*, Report Prepared for Portland Cement Association, PCA R&D Serial No. 1916, December 1992.

27. Wu, C.L., Mack, J.W., Okamoto, P.A., and Packard, R.G., *Prediction of Faulting of Joints in Concrete Pavements*, Proceedings of the Fifth International Conference on Concrete Pavement Design and Rehabilitation, Purdue University, Indiana, April, 1993.

APPENDIX A – DATA BASE FOR ANALYSIS OF TRANSVERSE CRACKING (GPS-3 DATA)

State	SHRP_ID	% slabs cracked	Age year	MR psi	Dslab in	Eslab, 10^6 psi	Poisson's ratio	Thermal expansion coef., /F	Subgrade k-value psi	Slab length, ft
5	3011	0	11.6	607	10.0	4.0	0.15	5.55E-6	222	15
6	3030	21.7	19.2	609	8.5	3.9	0.14	5.55E-6	276	15.5
6	3042	12.4	16.5	714	8.8	3.5	0.13	5.55E-6	143	15.5
8	3032	37.2	16.3	615	8.0	3.8	0.20	5.55E-6	394	15.5
12	3804	62.4	6.3	553	12.0	4.0	0.19	5.55E-6	211	19.5
12	3811	64	18.6	502	9.4	3.1	0.17	5.55E-6	300	20
12	4000	0	18.4	469	8.1	3.6	0.15	5.55E-6	158	20
12	4057	0	4.7	537	13.3	3.8	0.17	5.55E-6	354	15.5
12	4059	0	4.0	765	6.0	4.4	0.20	5.55E-6	303	14
12	4109	0	4.0	629	7.0	4.2	0.20	5.55E-6	300	14
12	4138	16	18.4	480	8.0	3.3	0.20	5.55E-6	182	20
13	3015	0	15.2	679	10.0	3.9	0.20	5.55E-6	243	20
13	3018	3.9	21.3	507	9.9	2.0	0.13	5.55E-6	201	19.5
18	3002	0	19.5	674	9.5	5.7	0.18	5.55E-6	147	15.5
18	3003	0	16.3	584	10.1	4.8	0.20	5.55E-6	176	20
18	3030	0	13.6	700	8.0	4.0	0.20	5.55E-6	226	15.5
18	3031	0	18.0	558	10.2	4.9	0.20	5.55E-6	139	15.5
19	3006	16	18.9	655	8.5	3.7	0.20	5.55E-6	95	20
19	3009	8	17.8	576	10.6	4.5	0.20	5.55E-6	135	20
19	3028	0	9.8	654	9.5	3.7	0.20	5.55E-6	106	20
20	3013	0	10.7	520	10.2	4.3	0.16	5.55E-6	304	15
20	3015	0	3.6	515	9.2	4.2	0.20	5.55E-6	129	15
21	3016	0	9.2	640	11.7	5.1	0.18	5.55E-6	174	15
26	3068	0	14.6	650	9.0	4.0	0.20	5.55E-6	300	15.5
26	3069	0	19.9	650	9.0	4.0	0.20	5.55E-6	165	14.5
27	3003	0	3.7	579	7.6	5.0	0.20	5.55E-6	78	15
27	3013	0	3.0	719	8.0	5.5	0.14	5.55E-6	72	15
29	5393	48	31.2	650	8.0	4.0	0.20	5.55E-6	88	30
31	3018	0	10.0	650	12.0	4.0	0.20	5.55E-6	159	15.5
31	3023	65.1	11.3	556	11.9	3.8	0.16	5.55E-6	167	15.5
31	3028	0	14.4	550	8.4	4.9	0.20	5.55E-6	110	15.5
31	3033	3.1	7.1	650	9.0	4.0	0.20	5.55E-6	132	15.5
32	3010	3.1	11.9	606	9.7	3.4	0.17	5.55E-6	105	15.5
32	3013	21.7	12.9	579	8.3	5.4	0.19	5.55E-6	323	15.5
38	3005	0	8.3	587	8.0	4.8	0.14	5.55E-6	83	13.8
38	3006	0	7.8	620	8.4	5.0	0.13	5.55E-6	125	14
40	4160	0	15.4	650	9.0	4.0	0.20	5.55E-6	110	15
40	4162	0	9.4	650	9.0	4.0	0.20	5.55E-6	118	15
42	3044	0	4.6	580	12.7	3.4	0.16	5.55E-6	505	20
46	3012	3	12.1	555	10.1	4.9	0.19	5.55E-6	240	15
53	3011	0	12.1	784	9.0	4.0	0.20	5.55E-6	180	11.4
53	3013	0	23.9	650	7.8	4.0	0.20	5.55E-6	159	15.5
53	3014	0	12.2	770	10.4	4.7	0.19	5.55E-6	108	11.5
53	3812	0	24.3	540	9.0	4.0	0.20	5.55E-6	195	15
53	3813	9.3	29.3	650	7.8	4.0	0.20	5.55E-6	89	15.5
83	3802	0	9.8	618	9.8	4.7	0.20	5.55E-6	88	15
89	3015	0	10.8	655	8.0	4.0	0.20	5.55E-6	73	16
89	3016	0	12.7	585	8.6	4.6	0.20	5.55E-6	89	16

State	SHRP_ID	Widened lane? (Yor N)	If widened distance-to-edge in	Tied shoulder? (Yor N)	If tied, AGG/kl	Base stabilized? (Yor N)	Base bonded? (U or B)	Dbase in	Ebase, psi
5	3011		0	N	0	Y	U	6.9	1000000
6	3030		0	Y	0.1	Y	U	4.3	1000000
6	3042		0	N	0	Y	U	5.5	1000000
8	3032		0	Y	0.1	Y	U	5.0	2000000
12	3804		0	N	0	Y	U	7.6	2000000
12	3811		0	N	0	Y	U	7.6	200000
12	4000		0	N	0	Y	U	5.7	200000
12	4057		0	N	0	N		7.0	20000
12	4059		0	Y	0.1	N		9.8	200000
12	4109		0	Y	0.1	N		9.8	200000
12	4138		0	Y	0.1	Y	U	5.9	200000
13	3015		0	Y	0.1	Y	U	6.0	200000
13	3018		0	Y	0.1	Y	U	6.8	1000000
18	3002		0	N	0	N		7.0	30000
18	3003		0	Y	0.1	Y	U	6.5	100000
18	3030		0	Y	0.1	Y	U	5.4	450000
18	3031		0	N	0	Y	U	5.6	450000
19	3006		0	N	0	Y	U	5.0	1000000
19	3009		0	Y	0.1	Y	U	5.7	200000
19	3028		0	Y	0.1	Y	U	5.0	2000000
20	3013		0	Y	0.1	Y	U	5.0	1000000
20	3015		0	N	0	Y	U	5.2	450000
21	3016		0	Y	0.1	N		7.0	30000
26	3068		0	N	0	Y	U	5.0	450000
26	3069		0	Y	0.1	Y	U	5.0	200000
27	3003	Y	24	N	0	N		6.0	30000
27	3013	Y	24	Y	0.1	N		6.0	30000
29	5393		0	N	0	N		4.0	30000
31	3018		0	Y	0.1	Y	U	6.0	200000
31	3023		0	N	0	Y	U	5.0	1000000
31	3028		0	Y	0.1	Y	U	4.0	100000
31	3033		0	Y	0.1	Y	U	5.8	450000
32	3010		0	Y	0.1	Y	U	6.6	1000000
32	3013		0	Y	0.1	Y	U	4.7	1000000
38	3005		0	N	0	N		3.0	30000
38	3006		0	Y	0.1	N		5.0	30000
40	4160		0	N	0	Y	U	4.0	0
40	4162		0	N	0	Y	U	4.0	450000
42	3044		0	Y	0.1	N		9.0	30000
46	3012		0	Y	0.1	N		5.0	30000
53	3011		0	N	0	N		5.8	30000
53	3013		0	Y	0.1	N		4.0	30000
53	3014		0	N	0	N		6.0	30000
53	3812		0	N	0	N		3.0	30000
53	3813		0	N	0	N		3.4	30000
83	3802		0	N	0	N		7.0	30000
89	3015		0	N	0	N		10.0	30000
89	3016		0	N	0	N		10.0	30000